The Graduate Institute of Sciences and Engineering

M.Sc. Thesis in Electrical and Computer Engineering

DESIGN AND FABRICATION OF OPTICAL ISOLATORS FOR PHOTONIC INTEGRATED CIRCUITS

by

Murat SERHATLIOĞLU

August 2014
Kayseri, Turkey

DESIGN AND FABRICATION OF OPTICAL ISOLATORS FOR PHOTONIC INTEGRATED CIRCUITS

by

Murat SERHATLIOĞLU

A thesis submitted to

the Graduate Institute of Sciences and Engineering

of

Meliksah University

in partial fulfillment of the requirements for the degree of

Master of Science

in

Electrical and Computer Engineering

August 2014
Kayseri, TURKEY

APPROVAL PAGE

This is to certify that I have read the thesis entitled "**DESIGN AND FABRICATION OF OPTICAL ISOLATORS FOR PHOTONIC INTEGRATED CIRCUITS**" by **Murat Serhatlıoğlu** and that in my opinion it is fully adequate, in scope and quality, as a thesis for the degree of Master of Science in Electrical and Computer Engineering, the Graduate Institute of Science and Engineering, Melikşah University.

____

August 25, 2014, Assist. Prof. Dr. Gökhan ÖZGÜR
Supervisor

I certify that this thesis satisfies all the requirements as a thesis for the degree of Master of Science.

____

August 28, 2014, Assoc. Prof. Dr. İhsan Ö. BUCAK
Deputy Head of Department

Examining Committee Members

Title and Name		Approved
Assist. Prof. Dr. Gökhan ÖZGÜR	August 29, 2014	______________________
Assist. Prof. Dr. A. Esad ÖZMETİN	August 29, 2014	______________________
Assist. Prof. Dr. Mahmut KARAKAYA	August 29, 2014	______________________

It is approved that this thesis has been written in compliance with the formatting rules laid down by the Graduate Institute of Science and Engineering.

____

Prof. Dr. M. Halidun KELEŞTEMUR
Deputy Director

August 2014

DESIGN AND FABRICATION OF OPTICAL ISOLATORS FOR PHOTONIC INTEGRATED CIRCUITS

Murat SERHATLIOĞLU

M. S. Thesis – Electrical and Computer Engineering

August 2014

Supervisor: Assist. Prof. Dr. Gökhan ÖZGÜR

ABSTRACT

Recently, there has been extensive research on the integration of photonic devices. The optical isolators, which allows light only in one direction, are indispensable components in the integration of photonic devices formed by bringing many devices on a single chip.

In this thesis, waveguides containing silicon nitride (S_3N_4) and zinc oxide (ZnO) cores have been fabricated on silicon and glass wafers. These waveguides contain nickel (Ni) thin films or ZnO:Ni composite films exhibiting magneto-optic Kerr effect (MOKE) and the devices have been designed to utilize this effect to allow the light to propagate in one direction and to absorb the light in the reverse direction. Furthermore, waveguide polarizers, which are exploiting the difference in the effective indices of transverse electric (TE) and transverse magnetic (TM) modes, have been designed and fabricated. 1-D WAVEGUIDE and 2-D WMM mode solvers have been used to investigate the behavior of the modes propagating in the waveguides.

The mask sets have been designed for the fabrication processes; the layers that constitute the structures have been grown and optically characterized; devices have been fabricated in the cleanroom and tested on the coupling experiment setup established.

Waveguide polarizer devices have been tested and it shows that these devices allow light for TE modes, but they do not permit the TM mode light by attenuating it. The waveguide isolators were designed for TM mode light to observe change in light intensity under the magnetic field. However, the conditions to observe this effect could not be reached due to the tight requirements of layer parameters in the structure.

Keywords: Optical isolator, MOKE, waveguide, polarizer

TÜMLEŞİK FOTONİK DEVRELER İÇİN OPTİK İZOLATÖR TASARIM VE ÜRETİMİ

Murat SERHATLIOĞLU

Yüksek Lisans Tezi – Elektrik ve Bilgisayar Mühendisliği
Ağustos 2014

Tez Yöneticisi: Yrd. Doç. Dr. Gökhan ÖZGÜR

ÖZ

Son zamanlarda, fotonik tümleşik devreler üzerinde yapılan çalışmalar yoğunlaşmıştır. Birden çok aygıtın tem bir yonga üzerinde bir araya getirilmesi ile elde edilen bu yapılarda, ışığı tel yönlü iletmesinden dolayı optik izolatörler kaçınılmaz bileşenlerdir.

Bu çalışmada, silisyum ve cam üzerine oluşturulan silisyum nitrat (S_3N_4) ve çinko oksit (ZnO) öz tabakalar içeren dalga kılavuzları tasarlanmıştır. Bu yapılarda manyetooptik Kerr etkisi (MOKE) gösteren ince nikel (Ni) film ve ZnO:Ni kompozit malzemelerin etkilerinden yaralanarak ışığı tek yönlü ileten, fakat ters yönde soğuran dalga kılavuzları tasarlanmıştır. Ayrıca, dalga kılavuzlarında ilerleyen enine elektrik (TE) ve enine manyetik (TM) modlarının etkin indeks farkından yararlanılarak dalga kılavuzu polarizör tasarımı ve üretimi yapılmıştır. Dalga kılavuzunda ilerleyen modların davranışlarını incelemek için 1-D WAVEGUIDE ve 2-D WMM mode çözücüler kullanılmıştır. Aygıtların üretim aşamasında gerekli maskeler tasarlanmış, yapıyı oluşturan katmanlar büyütülmüş ve optik karakterizasyonları yapılmış, aygıtlar

temizoda ortamında üretilerek, kurmuş olduğumuz optik kuplaj düzeneğinde test edilmişlerdir.

Yapılan test çalışmalarının sonucunda, dalga kılavuzu optik polarizör yapının TE modunu ilettiği, fakat TM modunu soğurarak elediği görülmüştür. Optik izolatör dalga kılavuzlarının manyetik alan altında testlerinde, kılavuzda ilerleyen TM modu için fark görülmesi hedeflenmiş, fakat üretilen yapının katmanlarına ait parametrelerin çok sıkı kontrol edilememesinden dolayı, bu etkinin oluşacağı şartlar sağlanamamıştır

Anahtar Kelimeler: Optik izolatör, MOKE, dalga kılavuzu, polarizör

DEDICATION

This thesis dedicated to my parents for their endless support and patience during the forming phase of this thesis.

ACKNOWLEDGEMENT

I would like to thank to The Scientific and Technological Research Council of Turkey (TUBITAK) that supported this thesis under the project number 110E280.

I would like to express my gratitude to my supervisor Assist. Prof. Dr. Gökhan ÖZGÜR, whose help, stimulating suggestions and encouragement helped me during the course of research and writing of this thesis. I also would like to thank UNAM, National Nanotechnology and Research Center at Bilkent University staffs for supporting my research on my thesis. I would like to thank ERNAM, Nano Technology Research Center at Erciyes University for their support in the fabrication process

I also want to thank my research partner Mehmet Ali for his significant contributions to my research endeavors.

I express my thanks and appreciation to my family for their understanding, motivation and patience. Lastly, but in no sense the least, I am thankful to all colleagues and friends who made me stay at the university a memorable and valuable experience.

TABLE OF CONTENTS

ABSTRACT ... iii
ÖZ ... v
DEDICATION ... vii
ACKNOWLEDGEMENT ... viii
TABLE OF CONTENTS ... iix
LIST OF FIGURES ... xi
LIST OF TABLES ... xiii
LIST OF SYMBOLS AND ABBREVIATIONS ... xiv
CHAPTER 1 INTRODUCTION ... 1
1.1 Photonic Integrated Circuits (PICs) ... 1
1.2 Optical Isolators ... 1
1.3 Objective of Thesis ... 5
CHAPTER 2 BACKGROUND ... 6
2.1 Ferromagnetic Composite Layer (FCL) ... 6
2.2 Concept of Resonant Layer Effect ... 6
2.3 Loss Calculation for a Waveguide Optical Isolator ... 9
2.4 Basic Principles of Magneto-Optics ... 10
2.5 Magneto-Optic Kerr Effect (MOKE) ... 12
CHAPTER 3 OPTICAL WAVEGUIDE ... 16
3.1 Introduction to Optical Waveguides ... 16
3.2 Numerical Modelling of Optical Waveguides ... 17
3.2.1 Wave Matching Method (WMM) Mode Solver ... 18
CHAPTER 4 DESIGN, FABRICATION AND TEST OF DEVICES ... 20
4.1 Introduction ... 20
4.2 Single Mode Waveguide (SMW) with Zinc Oxide (ZnO) Core ... 21
4.2.1 Simulations of Waveguide ... 21
4.2.2 Mask Sections ... 24

4.2.3 Fabrication Steps 24
4.2.4 Experimental Findings 26
4.2.5 Results 27
4.3 Single Mode Waveguides with Si_3N_4 Core with Lossy Layer 27
4.3.1 Waveguide Simulations 28
4.3.2 Fabrication Steps 30
4.3.3 Experimental Findings 32
4.3.4 Results 34
4.4 Design of an Optical WG Isolator with Si_3N_4 Core and Nickel Layer 35
4.4.1 Waveguide Simulations 36
4.4.2 Fabrication Steps 37
4.4.3 Experimental Findings 39
4.4.4 Results 39
4.5 Design of an Optical WG Isolator with Si_3N_4 and ZnO:Ni Core 39
4.5.1 Waveguide Simulations 40
4.5.2 Mask Sections 41
4.5.3 Fabrication Steps 42
4.5.4 Experimental Findings 44
CHAPTER 5 TEST SETUP FOR OPTICAL ISOLATOR 45
5.1 Experimental Setup 45
CHAPTER 6 CONCLUSION 48
6.1 Descussion of the Results 48
APPENDIX A 50
APPENDIX B 52
REFERENCES 57

LIST OF FIGURES

FIGURE

1.1 Illustrative view of polarization dependent optical isolator.................................... 3

2.1 Single mode profile of optical waveguide (left) and RLE in FCL layer, fabricated at the top of waveguide (right) (n2 > n3 > n1)……………………………………….7

2.2 Refractive index profile of primary waveguide and RL in no interaction.............. 8

2.3 Refractive index profile of primary waveguide and RL in interaction................... 9

2.4 Magneto-optic effects 11

2.5 Geometries for magneto-optical Kerr effect, (a) polar Kerr effect; (b) longitudinal Kerr effect; and (c) transverse Kerr effect. M is the magnetization vector 11

2.6 The coordinate presentation of randomly magnetized magnetic medium 2 and non-magnetic medium 1... 12

3.1 A slab waveguide structure.. 16

3.2 A slab waveguide index profile (n1 > n2, n3) 16

3.3 Structure definition for WMM.. 18

4.1 Cross-sectional view of ZnO core single mode waveguide.................................. 22

4.2 TM mode near field intensity of ZnO based waveguide 22

4.3 Lateral TE mode near field intensity (calculated by effective index method)....... 23

4.4 2-D Intensity field plot of TM mode SMW (contour plot).................................. 23

4.5 2-D Intensity field plot of TM mode SMW 23

4.6 Representative Image of Projected Photolithography Mask................................. 24

4.7 Ridges on silicon substrate, defined by lithography (PR on top) 25

4.8 Constituted ridges on glass (left) and silicon (right) substrate (PR removed)....... 25

4.9 Coupled light on end facet of SM WG. 26

4.10 Light profiles from end facet of SM WG. When coupling starting (left), coupling moment (center), far field (right).. 27

4.11 Cross-sectional view of single mode waveguides with Si_3N_4 core 28

4.12 1-D simulation of TE mode near field intensity 29

4 13 1-D simulation of TM mode near field intensity 29
4.14 For TE and TM modes, optical losses of even and odd modes. 30
4.15 2 minute deep wet etching of Si in KOH solvent at 90 °C. 31
4.16 SiO_2 hard mask removed after 3-minute wet etching of Si. 31
4.17 100x microscope objective image of fabricated sample. 32
4.18 TE mode near field intensity of coupled light into waveguide (40x objective) 33
4.19 TE mode coupled into waveguide on fabrication completed sample (100x objective used to have better resolution) 34
4.20 TM mode coupled into waveguide for another device on fabrication completed sample (100x objective used) 34
4.21 Cross-sectional view of single mode waveguides with Si3N4 core 36
4.22 TM mode profile 37
4.23 20x microscope objective image of fabricated sample with four branches 38
4.24 100x microscope objective image one of the branches of the fabricated sample with Nickel on top.. 38
4.25 TE mode intensity profile coupled out of end facet of a device with four branches (40x image) 39
4.26 Two branch waveguide grown on silicon substrate, left branch is main bottom WG and right branch is ZnO:Ni WG on top 41
4.27 Optical intensity profile of TM mode for ZnO:Ni based WG 41
4.28 The main bottom waveguide structure with two branches on photo-mask 42
4.29 Patterned PR to form the 5 µm wide ridges on ZnO:Ni section 43
4.30 100x microscope objective image of one of the ridges of the fabricated device (Before PR removed after BOE etching) 43
4.31 100x microscope objective image of one of the ridges of the fabricated device (After PR removed and sample cleaned) 43
4.32 TE mode near field intensity profile of fabricated device with 100x microscope objective 44
5.1 Coupling setup front right view 46
5.2 Close up view to the sample vacuum holder, magnet holder, imaging and coupling objective lenses 46
5.3 Coupling setup 47
5.4 Close up view to the sample vacuum holder, magnet holder, imaging 47

LIST OF TABLES

TABLE

4.1 SMW on glass substrate at λ= 1310 nm 21

4.2 SMW on silicon substrate at λ= 1310 nm 21

4.3 Structure parameters of Si_3N_4 based optical isolator at λ = 1310 nm. 28

4.4 Structure parameters of Si_3N_4 based SMW at λ = 1310 nm 36

4.5 Structure parameters of Si_3N_4 and ZnO:Ni based SMW at λ = 1310 nm. 40

A.1 Growth parameters for SiO_2 and Si_3N_4 on PECVD 50

A.2 Co-Sputtering Parameter for ZnO:Ni 50

A.3 Wet etching parameters for fabricated materials 51

A.4 Dry etching parameters for SiO_2 on ICP 51

B.1 20 µm wide stripes on Mask - I 52

B.2 Trench section on Mask - II 52

B.3 5 nm deep - 7 µm wide Si_3N_4 etch section on Mask - II 53

B.4 Si_3N_4 protection and etch section on Mask - II 53

B.5 SiO_2 etch section on Mask - II 54

B.6 Nickel etch section on Mask - II 54

B.7 Trench section on Mask - III 55

B.8 5 nm deep - 7 µm wide Si_3N_4 etch section on Mask - III 55

B.9 ZnO:Ni protection and etch section on Mask - III 56

B.10 SiO_2 etch section on Mask - III 56

LIST OF SYMBOLS AND ABBREVIATIONS

SYMBOL / ABBREVIATION

EIC	Electronic Integrated Circuit
FCL	Ferromagnetic Composite Layer
FR	Faraday Rotation
ICP	Inductively Coupled Plasma
LD	Laser Diode
MCM	Magnetic Composite Material
MO	Magneto Optic
MOKE	Magneto-Optic Kerr Effect
MZI	Mach-Zhender Interferometer
PECVD	Plasma Enhanced Chemical Vapor Deposition
PIC	Photonic Integrated Circuit
PR	Photoresist
RLE	Resonant Layer Effect
SMW	Single Mode Waveguide
SOA	Semiconductor Optical Amplifier
TE	Transverse Electric
TM	Transverse Magnetic

WG	Waveguide
WMM	Wave Matching Method
Γ_{RL}	Confinement factor of light to resonant layer
θ_F	Faraday rotation angle
Q	Magneto-optic constant
n_C	Refractive index of cladding layer
n_{RL}	Refractive index of resonant layer
n_{WG}	Refractive index of waveguide core layer
n_{air}	Refractive index of air
N_{WG}	Effective index of waveguide
N_{WG}	Effective index of resonant layer
N_{WG}	Effective index of waveguide

CHAPTER 1

INTRODUCTION

1.1 Photonic Integrated Circuits (PICs)

Photonic devices use light instead of electrons to perform an optical function. Photonic integrated circuits (PICs) are devices which integrate multiple photonic devices and use the functionality of many optical devices on a single platform.

While Electronic integrated circuits (EICs) can integrate many transistors, capacitors and resistors on a single chip, a PIC integrates lasers, modulators, detectors, attenuators, multiplexers/demultiplexers, and amplifiers [1].

Nowadays, too much effort has been put on PICs since their ability of high data transfer capacity and functionality compared to EICs. Recent developments in nanostructures, metamaterials, and silicon technologies have expanded the range of possible functionalities for these highly integrated optical chips.

1.2 Optical Isolators

Reflection of light from the end faces of optical components is inevitable. Thus, protecting the optical light sources (like lasers) which are present in the optical systems is crucial since reflected light cause lack of stabilization on the oscillation of light sources. This is crucial for devices especially requiring long span lengths between transceiver pairs [2].

Optical isolators are magneto-optic devices, which are used in optical transmission systems for protecting optical light sources and active components. These

are optical components that, allows the light to pass only one way (ideally) as the diode counterpart in electronics

Although the integration of isolators have been realized commercially in the areas of microwave and millimeter waves, compact and low-cost integrated isolators have not appeared in the market yet [3].

The worldwide optical isolator consumption was led by Telecommunication applications in 2013 with a 70 percent market share or $349.7 million, and is forecasted to increase 19.6 percent to a value of $418.2 million in 2014 [2].

A major user-group within the specialty application category is R&D laboratories. Optical isolators are used for many purposes, such as noise reduction, medical imaging, pulse selection for mode locked lasers, sensing, regeneration switches, disc master, optical trapping, phase shifters, frequency modulation spectroscopy and general shuttering. The optical isolators are also used in sensing for industrial, structures and other many other communication product-oriented manufacturing and R&D tests [2].

Optical isolators divide into two main groups according to polarization dependency or independency. There are two types of operation principles for isolators; these are Faraday rotation effect and magneto-optic Kerr effect. The Faraday rotation effect discovered by Michael Faraday in 1842 is a non-reciprocal phenomenon since it is dependent on direction of the magnetic field [4].

In polarization dependent isolators, it is necessary to use input and output polarizers. In the forward direction, source light first pass through an input polarizer and it linearly polarized. Then it enters to the faraday rotator, which is a magneto-optic (MO) medium, providing 45 degree of polarization rotation whether clockwise or counter clockwise. A polarizer (analyzer) fixed to 45 degree at the output allows the source light to pass to the system. In the backward direction, 45 degree polarized light passes through the analyzer (now acts as input polarizer). While it is passing through faraday rotator, it gets further 45 degree rotation. When it meets the input polarizer (acting as output polarizer) it cannot pass through since the polarization plane has returned 90 degrees in total with respect to the polarization of the source light. The internal structure of an isolator device is shown in figure 1.1.

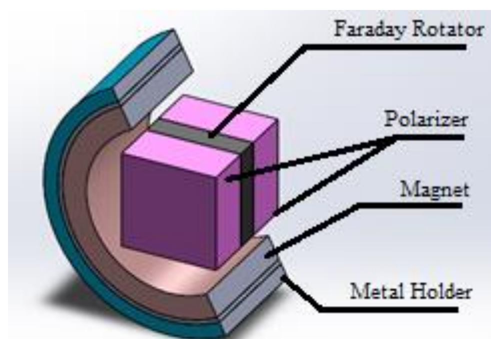

Figure 1.1: Illustrative view of polarization dependent optical isolator

Polarization dependent isolators are mostly used in free space optical systems, since it is hard to keep polarization in the fiber. For the bulk component isolators, garnets are used as a magneto optic layer, whereas an analyzer may not be used to minimize the device dimension. But as mentioned before, without analyzer it is not possible to perfectly guarantee that reflected light maintains the same polarization and it also is inevitable to have loss for back reflection.

For polarization independent isolators, birefringent lenses are used instead of polarizers. When the source light meets with first birefringent lens, it displaces into two directions. At the center of the isolator there are a faraday rotator and a half wave plate both of which provide 90 degree rotation in polarization plane for both directions. Separated light recombines into one once it passes through second birefringent lens. When the light reflects back it will be split into two and distracted from the light source

Integrated optical isolators started to be reported in 1970s. These bulk isolators used thick magneto-optical garnet films that were grown on garnet substrates [5].

Customary isolators based on Faraday rotation (FR) which requires complex structure and components. Several materials have been studied that have excellent magneto-optical activity, but also losses that are too high to allow sufficient light to transmit into the circuit [6]. Other materials have very low loss, but not enough MO activity for reasonably sized devices [7].

It is hard to integrate isolators with laser diodes (LD) because materials and device structure of conventional optical isolators are completely different from those of

waveguide devices on semiconductor substrates [8]. Although various configurations have been studied for waveguide isolators, they could not succeed to have effective isolators once compared to bulk isolators. To overcome these challenges, integrated optical waveguide isolators which utilize nonreciprocal phase shift have emerged. These structures do not require the struggles such as mode conversion and difficulty of phase matching condition as in the case of FR [9]. The nonreciprocal phase shift occurs in TM modes that travel in magneto-optic waveguides where the magnetization is aligned transversely to the light propagation direction in the film plane [10].

Mizumoto et al. [11] firstly characterized nonreciprocal propagation of YIG films. They used rare earth iron garnets as an optical isolator that is employing non-reciprocal phase shift [12]. Then, Yokoi et al. reported two papers (in one year intervals) that consist Mach Zehnder interferometer (MZI) isolator which experiences nonreciprocal effective index shift and requires wafer bonding on an InP substrate [13] - [14].

Ferromagnetic materials used in waveguide isolators firstly theoretically studied by Hammer et al. They showed that a nonreciprocal TE–TM mode converter can be obtained using a semiconductor waveguide covered by a Fe ferromagnetic layer with an alternatively reversing of magnetization direction. They have suffered from very high insertion loss [15].

Nonreciprocal loss type isolators were first reported by Zaets et al. [16]. They have offered semiconductor optical amplifier (SOA) covered by a ferromagnetic layer which has a large difference in values of loss/gain for modes propagating in the opposite directions when the magnetization is perpendicular to the light propagation direction and lies in the film plane. Thus, the amplifier covered by ferromagnetic can itself act as an optical isolator and they have reduced the insertion loss.

Even though using ferromagnetic layers with magneto-optic (MO) effect is a wise choice, isolators suffer from very high insertion losses. To compensate this loss, high gain SOAs can be used, but this introduces unwanted noise into the system.

Baba et al. demonstrated a new type of magnet-optic media composed of ferromagnetic metal island films on glass substrates. The optical loss of ferromagnetic metal island films was much lower than that of conventional ultra-thin films with

continuous structure. Even though these films exhibit strong Faraday effect, it is not convenient to use this composite layer as a core of a waveguide isolator. [17].

An optical isolator which use a magnetic composite material (MCM) having ferromagnetic-composite layer (FCL) was first proposed and reported by Hammer [18]. The optical isolator consists of a core, a cladding, and a MCM which is placed close to core on top of the cladding. Hammer et al. also proposed a type of isolator and other optical waveguide devices that utilizes the concept of resonant layer effect (RLE) [18].

1.3 Objective of Thesis

This thesis aims to present a low-loss optical silicon based low-cost integratable waveguide isolator which uses the FCL and RLE concepts. The theoretical background on the concepts of the proposed isolator is given in chapter 2. In chapter 3, the optical simulation models and software used in the work are presented. Chapter 4 consists of the design, fabrication and test results of the devices made for this work. Chapter 5 concludes the findings and mentions the future work.

CHAPTER 2

BACKGROUND

2.1 Ferromagnetic Composite Layer (FCL)

MO effect plays an important role on optical communication systems. There are some difficulties of fabrication of materials like yttrium iron garnet (YIG), gallium gadolinium garnet (GGG) even though they have good MO properties because these materials have to be grown epitaxially. On the other hand, thin ferromagnetic films such as nickel (Ni), iron (Fe) has strong MO effects and are easy to fabricate on glass or semiconductor substrates, but they have very large optical losses.

The concept of using composite materials which consist the mixture of lossless semiconductor material like zinc oxide (ZnO), silicon nitride (Si_3N_4), silicon (Si) embedded with ferromagnetic material, like nickel (Ni), iron (Fe), cobalt (Co) can be a convenient way to have magneto optical media with low optical losses.

The purposed devices in this work utilize a FCL which consist ZnO as lossless high index material and nickel as ferromagnetic material. The nickel ratio in the composite layer is around 5%. The optical loss of FCL is measured to be around 64.27/cm which is four orders of magnitude lower than bulk Ni material.

2.2 Concept of Resonant Layer Effect

In a single mode optical waveguide, the fundamental has a peak in the high index core of waveguide and it tails extend to low index surrounding layers as shown in Figure 2.1 (left). When another high index layer is placed onto the cladding, a secondary peak of the fundamental mode can appear in this high-index layer when the thickness is within a certain range as shown in Figure 2.1 (right) [2].

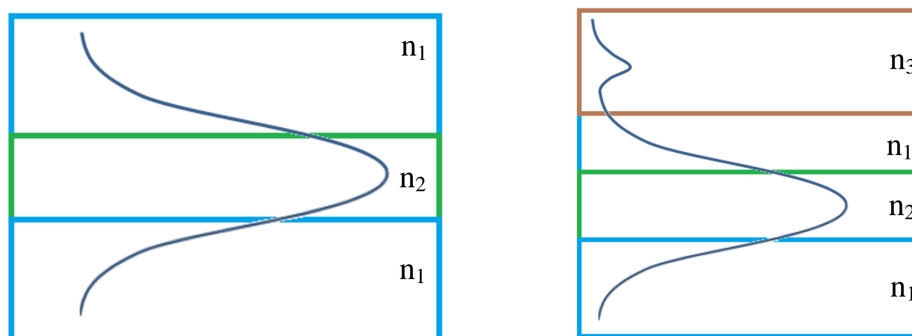

Figure 2.1: Single mode profile of optical waveguide (left) and RLE in FCL layer, fabricated at top of waveguide (right) (n2 > n3 > n1)

Instead of using lossy magneto-optic medium as the core of a waveguide where is most of the mode is guided, it is preferred to have a lossy layer on top of cladding which is far from center of waveguide. Bu applying an external magnetic field, the propagation constant of the mode changes for opposite directions due to the magneto-optic Kerr effect. If the FCL location, thickness and refractive index are properly chosen, a high secondary field peak is observed in the FCL for one direction and a lower peak appears in this layer. This phenomenon is called resonant layer effect [19]. When this condition is satisfied, a small change in the propagation constant of the guided mode will result in large changes in the confinement factor of the resonant layer [3].

Consider two separate waveguides which both have high index materials surrounded by cladding layers as shown in figure 2.2. If both waveguide are close enough to interact with each other, there will be field energy distribution between two dissimilar waveguides. Whether the most of the field will be carried in the second or first waveguide depends on the thickness and refractive index of layers. First waveguide consisting of layers 1, 2 and 3 in figure 2.3 should carry the most of the field and some light is confined to the second waveguide which consists of layers 3, 4 and 5.

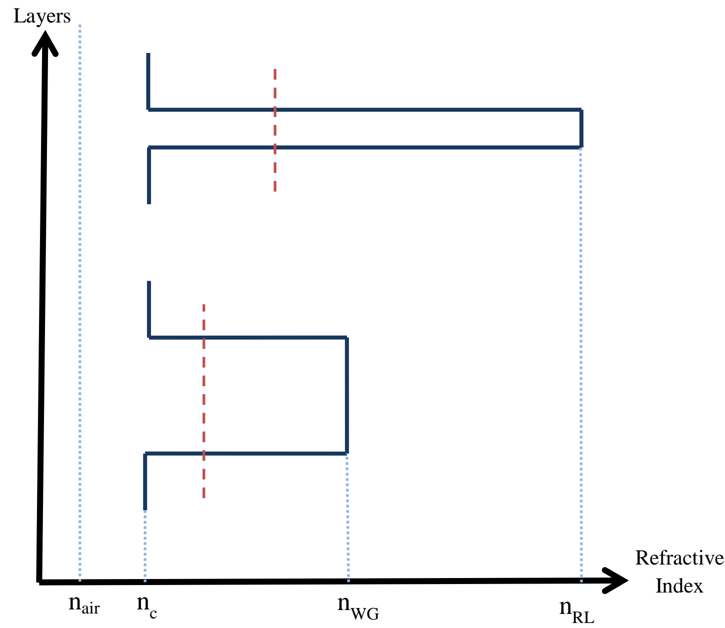

Figure 2.2: Refractive index profile of primary waveguide and RL in no interaction

The proper thickness of RL may be found by the following steps: Take the primary waveguide and consider it has an infinitely thick substrate and cladding which refractive index is n_C and core layer (layer 2 in figure 2.3). The core has refractive index n_{WG} which is greater than n_C. Then, find the effective index N_{WG} of primary waveguide of the lowest order mode. Also, for the secondary waveguide which has the same index of n_C at the bottom, refractive index of n_{RL} which is the index of RL layer at the core and as a top layer which might be the same as bottom or other material which has the lower index than core of secondary waveguide, the same method is applied and effective index of N_{RL} calculated as a function of the thickness of RL (t_{RL}).

When the effective indices become equal for two sub-waveguides ($N_{RL} = N_{WG}$) in the structure, both waveguides come to resonance. If there is no matching between two effective indices, then a matching point may be obtained by changing other parameters (such as t_{RL}, t_{WG}, t_C).

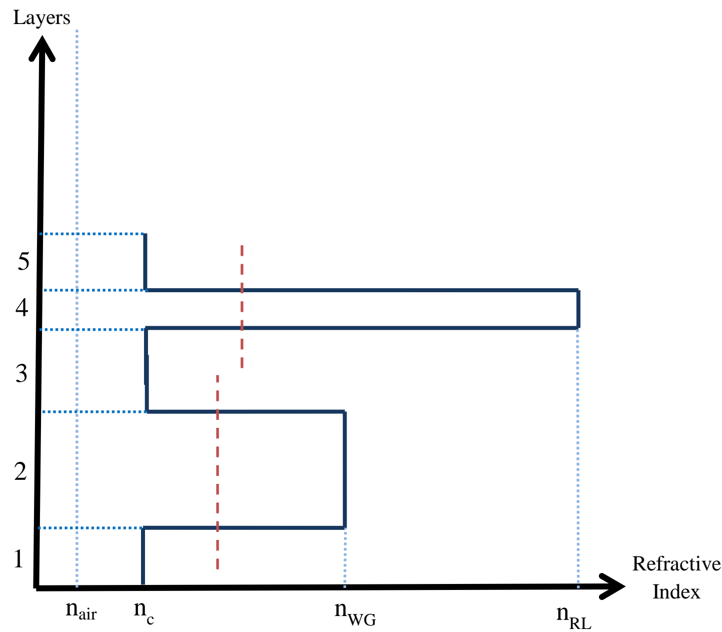

Figure 2.3: Refractive index profile of primary waveguide and RL in interaction

When two effective indices are matched, the confinement factor in the RL (Γ_{RL}) can be found to determine the effect and loss due to this layer. The thickness of the cladding t_C has influence the value of Γ_{RL} and also it has a secondary influence on the optimum thickness of the RL. In many cases, t_C is chosen such that confinement factor Γ_{RL} is less than about 0.25, which implies that less than 25% of the field intensity is confined to the RL [3].

2.3 Loss Calculation for a Waveguide Optical Isolator

Insertion loss is the loss on forward propagation direction and the loss on the backward direction is referred as isolation. The isolation-to-loss ratio is the ratio of isolation to insertion loss. Changing the direction of light can be considered the as changing the direction of externally applied magnetic field. A propagating plane wave in $+z$ direction with a complex propagation constant γ and power loss are defined in equations 2.1 and 2.2, respectively.

$$\gamma = \alpha + j\beta \qquad 2.1$$

$$\exp(-\gamma z) \qquad 2.2$$

The optical power loss coefficient is defined in equation 2.3 where is the k is the absorption coefficient of the medium,

$$\alpha\ (cm^{-1}) = \frac{4\pi k}{\lambda} \qquad 2.3$$

.

The optical power loss (cm^{-1}) is related to the imaginary part of complex refractive index and is defined in equation 2.4. The loss in decibels per centimeter is defined in the equation 2.5.

$$Loss = \exp(-\frac{4\pi k}{\lambda} z) \qquad 2.4$$

$$Loss\ ({}^{db}/_{cm}) = -10\log[\exp(-\frac{4\pi k}{\lambda} z)] \qquad 2.5$$

where z is the distance traveled.

2.4 Basic Principles of Magneto-Optics

Magneto optical effects are appeared when the linearly polarized light interacts with magnetic medium. There are two famous types of phenomena according to magneto-optic effects which are Faraday and Kerr effects. Faraday effect, which is defined passing of light, through a magnetized material firstly investigated by Michael Faraday in 1845 [20]. The Kerr effect, which occurs when the light is reflected from the magnetized material, was found by John Kerr in 1875 [21].

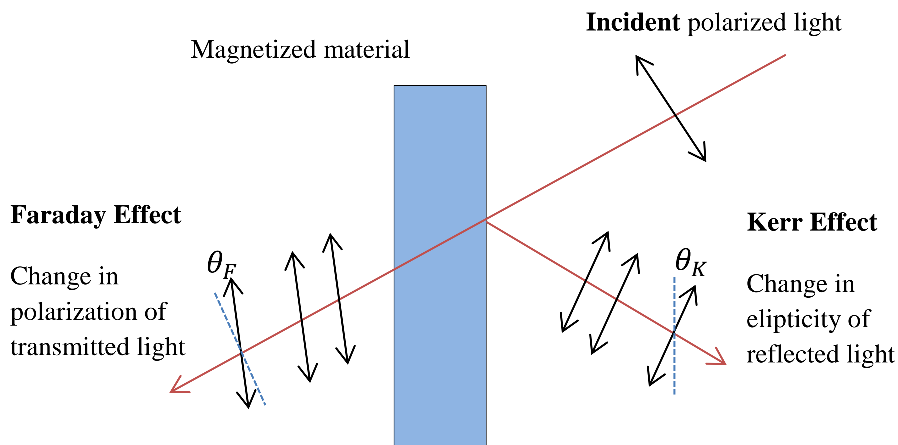

Figure 2.4: Magneto-optic effects

Conventionally, there are three types of MO effects which can be specified by the direction of the magnetization vector according to the reflection surface and plane of incidence light. Kerr effect (KE) is called polar when the magnetization is perpendicular to the reflection surface and parallel to the plane of incidence, longitudinal when the magnetization is both parallel to the plane of incidence and the reflection surface, transversal when the magnetization vector is parallel to the reflection surface and perpendicular to the plane of incidence.

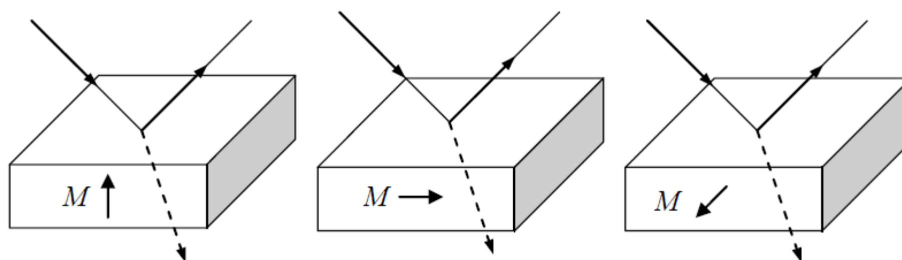

Figure 2.5: Geometries for polar, longitudinal, and transverse magneto-optic Kerr effect. (M is the magnetization) [3]

While describing the Faraday rotation, the MO constant, Q is can be found by Faraday rotation θ_F which is the ratio of the rotation angle of polarization status and the distance covered by the light wave within the material [3].

$$\theta_F = \frac{\pi n Q}{\lambda} \qquad 2.6$$

The equation above shows the relation between MO constant Q and the Faraday rotation θ_F. In equation 2.6, n is the refractive index of material and λ is the free space of wavelength [22].

2.5 Magneto-Optic Kerr Effect (MOKE)

If there are backside reflections from bulk materials or deposited films, it is called thin films and underlying layer should be taking into account for MOKE measurement. Also thick film MOKE formulism is used. Otherwise the film is considered thick, and then thick film formulism is valid for measurements [23].

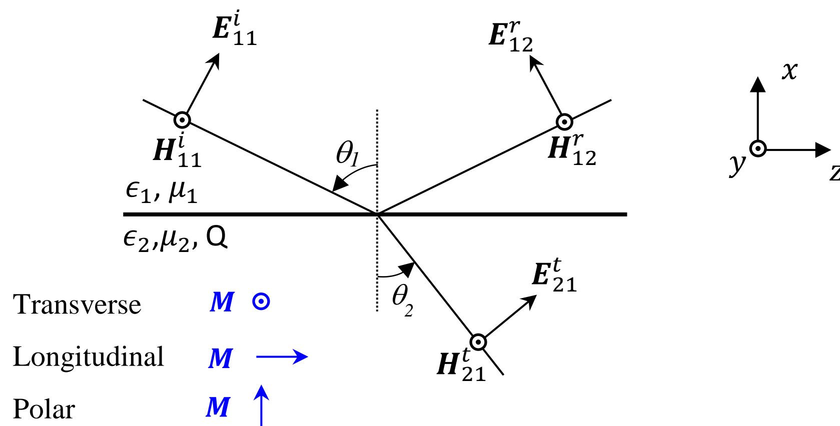

Figure 2.6: The coordinate presentation of randomly magnetized magnetic medium 2 and non-magnetic medium 1

MOKE calculations for optically thin films explained in detail in reference [24]. General form of dielectric tensor of any medium is,

$$\epsilon = \begin{bmatrix} \epsilon_{xx} & \epsilon_{xy} & \epsilon_{xz} \\ \epsilon_{yx} & \epsilon_{yy} & \epsilon_{yz} \\ \epsilon_{zx} & \epsilon_{zy} & \epsilon_{zz} \end{bmatrix} \quad 2.7$$

since, ϵ_{xx}, ϵ_{yy}, are ϵ_{zz} are very close to each other, they can assumed to be equal. In other words:

$$\epsilon_{xx} = \epsilon_{yy} = \epsilon_{zz} \quad 2.8$$

The MO constant Q belongs to magnetic material. It is defined in off-diagonal terms in the dielectric tensor.

$$Q = i\frac{\epsilon_{xy}}{\epsilon_{xx}} \quad 2.9$$

The gyromagnetic effects are negligibly small due to the inertia of the magnetization process at optical frequencies. Therefore, the relative permeability of the medium is taken as unity, $\mu \approx 1$ [3]. Dielectric tensor under arbitrary direction of magnetization for incident light which is passing from non-magnetic media 1 to magnetic media 2 is given in equation 2.10.

$$\epsilon = \epsilon_{xx} \begin{bmatrix} 1 & iQm_x & iQm_y \\ -iQm_x & 1 & iQm_z \\ -iQm_y & -iQm_z & 1 \end{bmatrix} \quad 2.10$$

where m_x, m_y ve m_z are the direction cosines of magnetization vector M. When Maxwell's equations are solved with the dielectric tensor, Fresnel reflection coefficient matrix can be achieved as,

$$R = \begin{bmatrix} r_{pp} & r_{ps} \\ r_{sp} & r_{ss} \end{bmatrix} \quad 2.11$$

where r_{ij} is the ratio of the incident j polarized electric field to the reflected i polarized electric field and they are given as [24] - [26].

$$r_{pp} = \frac{E_{pp}^{r}}{E_{pp}^{i}} \quad 2.12$$

$$r_{sp} = \frac{E_{ss}^{r}}{E_{pp}^{i}} \quad 2.13$$

$$r_{ps} = \frac{E_{pp}^{r}}{E_{ss}^{i}} \quad 2.14$$

$$r_{ss} = \frac{E_{ss}^{r}}{E_{ss}^{i}} \quad 2.15$$

$$\mathrm{r_{pp}} = \frac{n_2 \cos\theta_1 - n_1 \cos\theta_2}{n_2 \cos\theta_1 + n_1 \cos\theta_2} + \frac{i2n_1 n_2 Q m_y \sin\theta_2 \cos\theta_1}{n_2 \cos\theta_1 + n_1 \cos\theta_2} \quad 2.16$$

$$\mathrm{r}_{sp} = \frac{i n_1 n_2 Q (m_z \sin\theta_2 - m_x \cos\theta_2)\cos\theta_1}{(n_2 \cos\theta_1 + n_1 \cos\theta_2)(n_1 \cos\theta_1 + n_2 \cos\theta_2)\cos\theta_2} \quad 2.17$$

$$\mathrm{r_{ss}} = \frac{n_1 \cos\theta_1 - n_2 \cos\theta_2}{n_1 \cos\theta_1 + n_2 \cos\theta_2} \quad 2.18$$

$$\mathrm{r}_{ps} = \frac{i n_1 n_2 Q (m_z \sin\theta_2 + m_x \cos\theta_2)\cos\theta_1}{(n_2 \cos\theta_1 + n_1 \cos\theta_2)(n_1 \cos\theta_1 + n_2 \cos\theta_2)\cos\theta_2} \quad 2.19$$

where θ_1, n_1, and n_2 are the angle of incidence, the refractive index of the nonmagnetic medium 1, and that of the magnetic medium 2, respectively.

These equations are valid within the first-order approximation of the magneto-optical constant Q and the complex refractive angle θ_2 in the magnetic medium 2 is determined by Snell's law [24].

When the magnetization direction is defined, the other direction cosines will be equal to zero. So, the dielectric tensor will be simplified to one direction cosine which is for the chosen magnetized direction for incident light. They can be categorized as

- Polar Magnetization; $m_x = 1, m_y = 0, m_z = 0$
- Longitudinal Magnetization; $m_z = 1,\ m_x = 0,\ m_y = 0$
- Transverse Magnetization; $m_y = 1, m_x = 0, m_z = 0$

For transverse MOKE (T-MOKE) case ($m_y = 1, m_x = 0, m_z = 0$), only r_{pp} has the term of Q and while r_{ss} does not depent on it. Also, r_{ps} and r_{sp} are equal to zero. Therefore, the magneto-optic effect will be observed only for p polarized (TM mode) light and there will be no power transfer from p to s or vice versa:

$$r_{pp} = \frac{n_2 \cos\theta_1 - n_1 \cos\theta_2}{n_2 \cos\theta_1 + n_1 \cos\theta_2} + \frac{i2n_1 n_2 \sin\theta_2 \cos\theta_1 Q}{n_2 \cos\theta_1 + n_1 \cos\theta_2}, \quad 2.20$$

$$r_{sp} = 0, \quad 2.21$$

$$r_{ss} = \frac{n_1 \cos\theta_1 - n_2 \cos\theta_2}{n_1 \cos\theta_1 + n_2 \cos\theta_2}, \quad 2.22$$

$$r_{ps} = 0. \quad 2.23$$

CHAPTER 3

OPTICAL WAVEGUIDE

3.1 Introduction to Optical Waveguides

Dielectric waveguides basically defines with, longitudinally extended high-index optical medium which is transversely surrounded by low-index media. A guided optical wave propagates along longitudinal direction in dielectric waveguide [27]. An example of slab waveguide and its refractive index profile is given in figure 3.1 and figure 3.2.

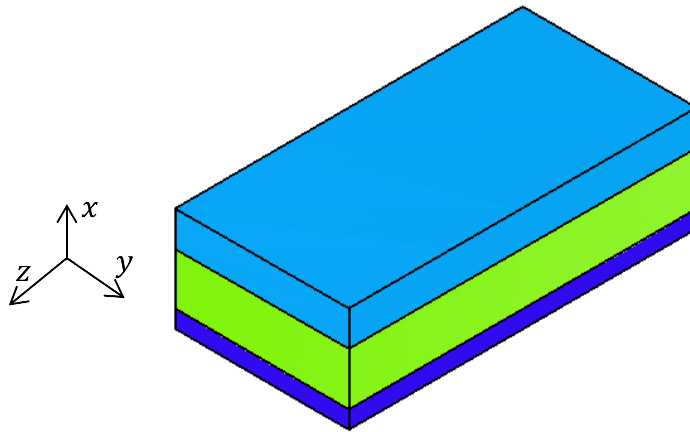

Figure 3.1: A slab waveguide structure

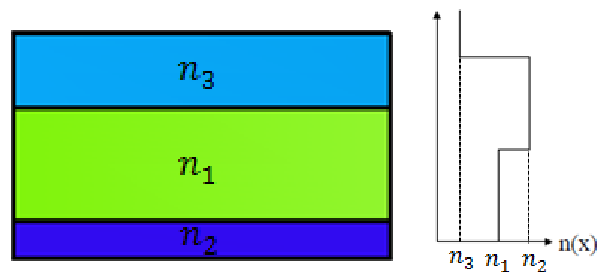

Figure 3.2: A slab waveguide index profile ($n_1 > n_2$, n_3)

Optical light is defined with “mode” definition in optical waveguides. A waveguide mode is a transverse field pattern whose amplitude and polarization profiles remain constant along the longitudinal z coordinate. Therefore the electric and magnetic fields of a mode can be written as following;

$$E_v(r,t) = E_v(x,y) \exp i(\beta_v z - \omega t) \quad 3.1.1$$

$$H_v(r,t) = H_v(x,y) \exp i(\beta_v z - \omega t) \quad 3.1.2$$

where v is the mode index, $E_v(x,y)$ and $H_v(x,y)$are the mode field profiles and β_v is the propagation constant of mode.

3.2 Numerical Modelling of Optical Waveguides

For ideal simple waveguide configurations, modes and propagation constant can be found analytically. However, for realistic waveguides, numerical calculations plays important role because they contain many layers. Fabrication tolerances and material losses can be crucial to determine waveguide modes. Depending on the waveguide parameters, only a single mode or more than one mode may be supported by waveguide.

Mode solvers are based on several numerical techniques. Some of the tools can simultaneously be used as mode solvers and as wave propagators (Transfer-Matrix Method, Eigenmode Expansion Method, Beam Propagation Method, Finite Element Method), while others are mode solvers only (Plane Wave Expansion Method, Multipole Method, Source Model Technique). While some numerical methods, such as the Finite Element Method, the Plane Wave Expansion Method, the Beam Propagation Method-based mode solvers, the Film Mode Matching Method, and the Finite-Difference Method, can be used for finding modes of the arbitrary cross-section and refractive index profile waveguides, others are more specialized [28]. Some mode solvers include software packages which consist from multiple mode solving techniques and numerical approaches.

3.2.1 Wave Matching Method (WMM) Mode Solver

WMM is open source software which is developed by Dr. Manfred Hammer. It is a quasi-analytic mode solver for rectangular dielectric integrated optical waveguide channels (three-dimensional configurations with two dimensional cross sections) based on wave matching method [29]. WMM is an approach for calculating the guided modes in waveguides which are has the 2-dimensional rectangular shape.

For solving the mode problems, on each region with constant refractive index a set of reasonable solutions to the basic wave equation is selected first and then the boundary conditions for dielectric interfaces combine fields on adjacent regions to a system of linear equations and as a last step, its appeared solutions yield propagation constants and mode profiles [29].

WMM yields semi-analytical mode field representations which are defined on the entire plane of the waveguide cross section. The fields are therefore perfectly suited for further processing, for instance in the framework of propagating mode analysis, coupled mode theory etc. While defining a waveguide to the WMM mode solver it assumes for cartesian coordinate system by the axes denoted by x, y and z. The structure is defined with x and y axes as shown in figure 3.3.

Layers	Structure					Thickness (nm)
8	Air	Air	Air	Air	Air	Infinite
7	Air	Air	SiO2	Air	Air	300
6	SiO2	SiO2	SiO2	SiO2	SiO2	300
5	ZnO:Ni	ZnO:Ni	ZnO:Ni	ZnO:Ni	ZnO:Ni	436
4	SiO2	SiO2	SiO2	SiO2	SiO2	1450
3	SiO2	SiN	SiN	SiN	SiO2	5
2	SiN	SiN	SiN	SiN	SiN	475
1	SiO2	SiO2	SiO2	SiO2	SiO2	2000
0	Si	Si	Si	Si	Si	4500
Borders	-3.5um	-2.5um		2.5um	3.5um	

Figure 3.3: Structure definition for WMM

WMM mode solver, consist of C++ library files. It is supported by C++ language. It does not have any other user interface. In order to have visual outputs, extra software

like GNU plot or MATLAB is needed. Also, it can be work under Linux and DOS operating systems.

CHAPTER 4

DESIGN, FABRICATION AND TEST OF DEVICES

4.1 Introduction

Several waveguide designs have been implemented to demonstrate the behavior of the modes in the waveguides and interaction of these modes with lossy magneto-optic layers. The ferromagnetic layers used in the structures are thin Ni films and ZnO:Ni composite films. Some waveguide have two Si_3N_4 core layers with nickel films and other designs include two core layers, which are Si_3N_4 and ZnO:Ni. The fundamental mode of the structure propagates in the Si_3N_4 guiding layer and has an interaction with either nickel layer or ZnO:Ni composite layer to exhibit the magneto-optic effect.

Some academic 1-D and 2-D mode solvers has been used to simulate the structures to determine the mode profiles, effective indices, modal losses and interaction of mode with lossy magneto-optic layers. The films layers have been grown by various deposition techniques and optical parameters of these films have been characterized. The design structures have been fabricated by common microelectronic fabrication methods.

An optical coupling experiment has been setup to test the devices. This setup is used to launch the single mode light in to the guiding layer of the devices at the desired polarization (TE or TM). The light exiting the devices has been observed to inspect the mode profiles in the devices.

Using the structure parameters obtained from the optical characterization results, the devices have been designed by some software tools. Modal analysis and loss calculations have been implemented by using WAVEGUIDE and WMM mode solvers. In this section, the steps followed in the design of devices will be introduced.

4.2 Single Mode Waveguide (SMW) with Zinc Oxide (ZnO) Core

ZnO is a transparent material used for many optoelectronic applications and has higher refractive index than silica. The index difference between ZnO and silicon dioxide (SiO_2) makes it possible to have an optical waveguide.

4.2.1 Simulations of Waveguide

The cross section of targeted structure is given in figure 4.1. TE and TM modes of designed waveguide are calculated using the refractive index of fabricated layers is given tables 4.1 and 4.2.

Table 4.1: SMW on glass substrate at λ= 1310 nm

Layer	Refractive Index	Thickness(um)
Air	1.0	-
SiO_2	1.45	1.0
ZnO	1.9036	0.4
Borosilicate Glass	1.45	500

Table 4.2: SMW on silicon substrate at λ= 1310 nm

Layer	Refractive Index	Thickness(um)
Air	1.0	-
SiO_2	1.45	1.0
ZnO	1.9036	0.4
SiO_2	1.45	1.0
Silicon	3.45	500

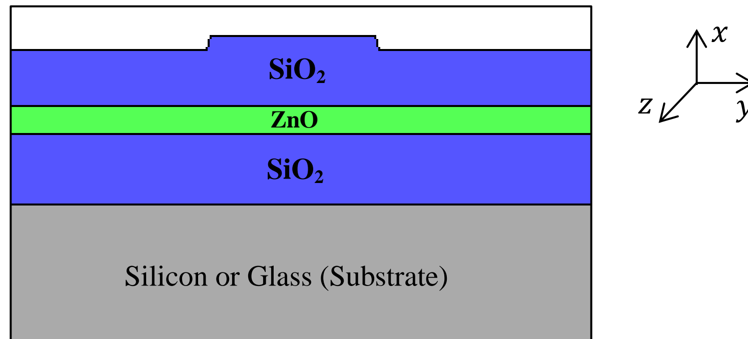

Figure 4.1: Cross-sectional view of ZnO core single mode waveguide.

Figure 4.2 shows the calculated near field intensity profile of TM mode and the lateral mode profile if shown in figure 4.3 using the 1-D mode solver WAVEGUIDE software. The same structure has also been using a 2-D mode solver called WMM. The calculated TM mode intensity profiles are given in figures 4.4 and 4.5

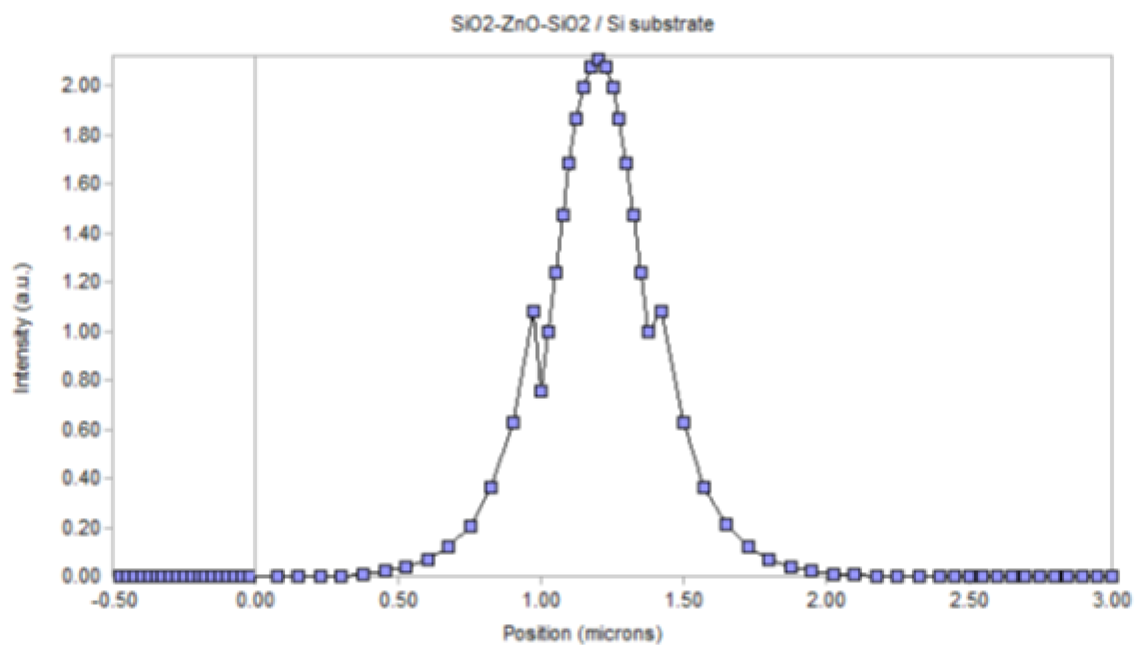

Figure 4.2: TM mode near field intensity of ZnO based waveguide

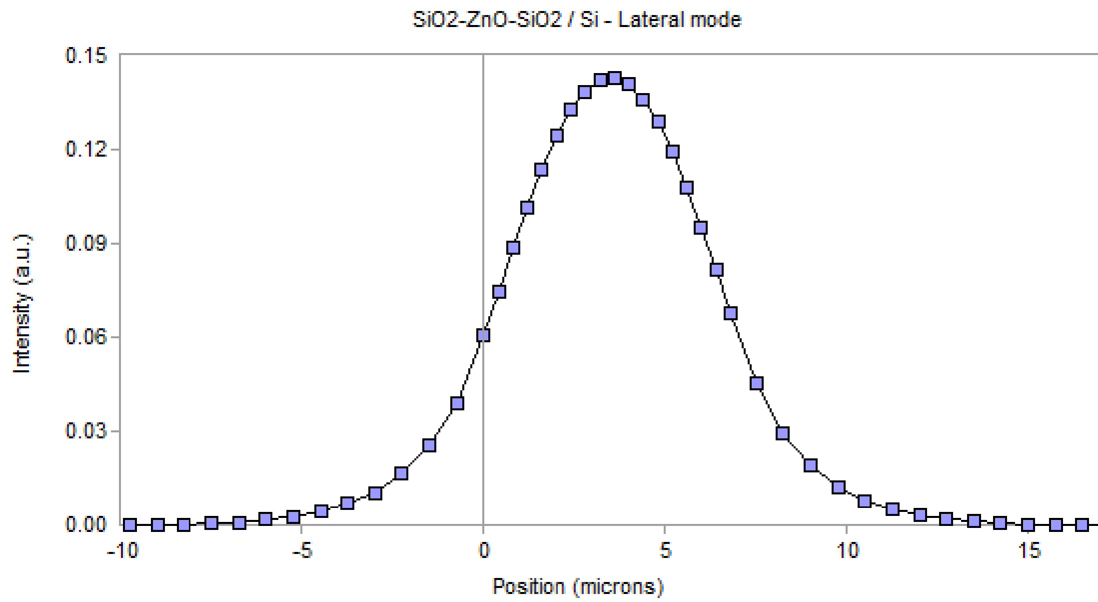

Figure 4.3: Lateral TE mode near field intensity (calculated by effective index method)

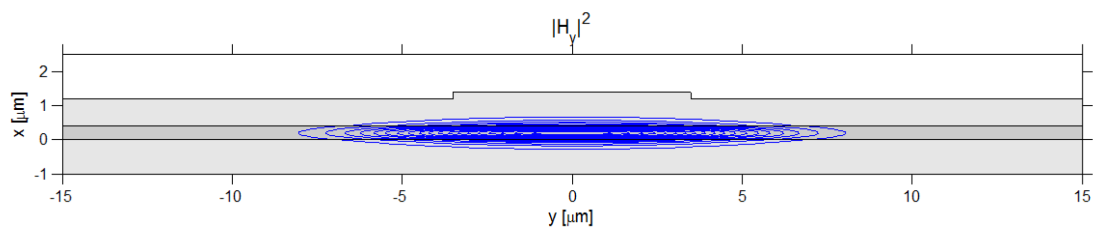

Figure 4.4: 2-D Intensity field plot of TM mode SMW (contour plot)

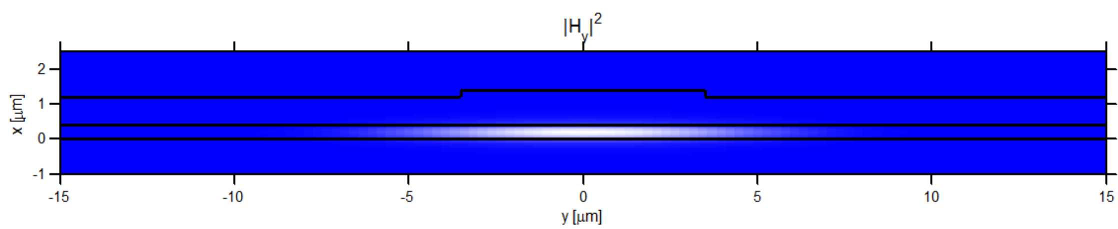

Figure 4.5: 2-D Intensity field plot of TM mode SMW

4.2.2 Mask Sections

The photolithography mask has been designed to fabricate the structure shown in figure 4.1. On the mask, there are 5, 7, 10, and 20 µm wide stripes as shown in figure 4.6 and figure 4.7. Mask also includes a section to define desired length for the rib waveguides, which can be 1, 2, 3, 5, and 7 mm long. The ridges have 250 µm spaces between them.

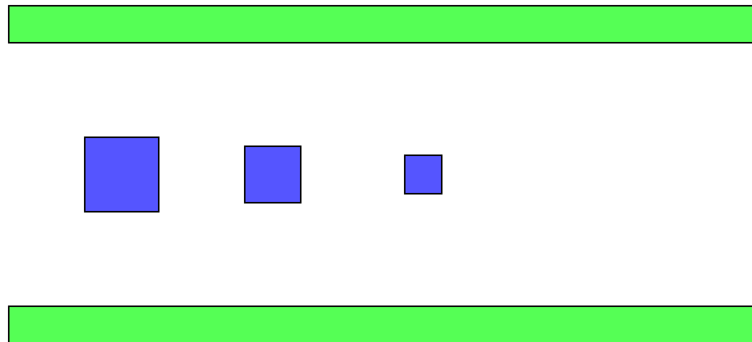

Figure 4.6: Representative Image of Projected Photolithography Mask

4.2.3 Fabrication Steps

ZnO films have been grown on glass substrates by RF magnetron sputtering. On the top of ZnO, SiO_2 is deposited by Plasma Enhanced Chemical Vapor Deposition (PECVD) method. 7-µm wide ridges patterned using photolithography mask on top SiO_2 layer with AZ5214 positive photoresist (PR). Rib waveguides have been formed by dry etching of SiO_2 with Inductively Coupled Plasma (ICP) at the desired thickness. PR selectivity to SiO_2 on ICP is 2:1, so for 200 nm of etching process, at least 400 nm of PR is required.

Figure 4.7: Ridges on silicon substrate, defined by lithography (PR on top)

After fabrication is complete, the devices have been dices at various lengths for testing. Figure 4.8 shows the final devices fabricated on glass (left) and silicon (right) substrates.

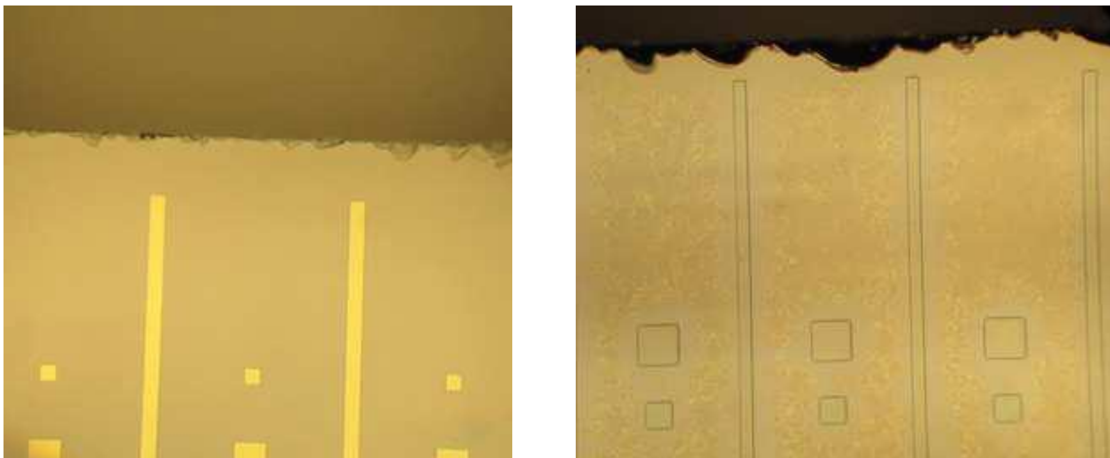

Figure 4.8: Constituted ridges on glass (left) and silicon (right) substrate (PR removed)

As seen from figure 4.8, some cracks on silicon substrate appeared after dicing, which are worse compared to glass substrate. This is due to the crystal orientation of silicon was <100>, but dicing was in <110> orientation. These devices were grinded

and polished in order to have smooth facets for light coupling into guiding layers and for imaging light leaving the devices.

4.2.4 Experimental Findings

Using the coupling setup described in Chapter 5, laser light have been coupled into the waveguides and the near field intensity has been observed at the other end facet. As seen in figure 4.9, coupled light coming out from the end facet of the device is a single mode. The light profile is elliptic, which is ~15 μm long horizontally and ~3 μm wide vertically. As compared the mode profiles shown in figures 4.2-4.3, the calculated and measured profiles are very similar.

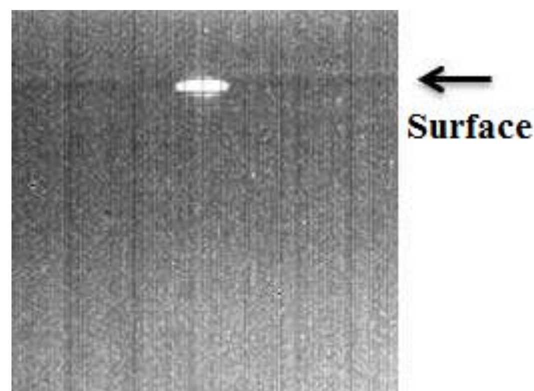

Figure 4.9: Coupled light on end facet of SMW

The coupling experiment results are indicated in figure 4.10. The left image shows that the coupling has just begun; while the middle one is when the coupling is perfect. The figure on the right shows the far-field profile of the coupled mode by focusing slightly away from the facet.

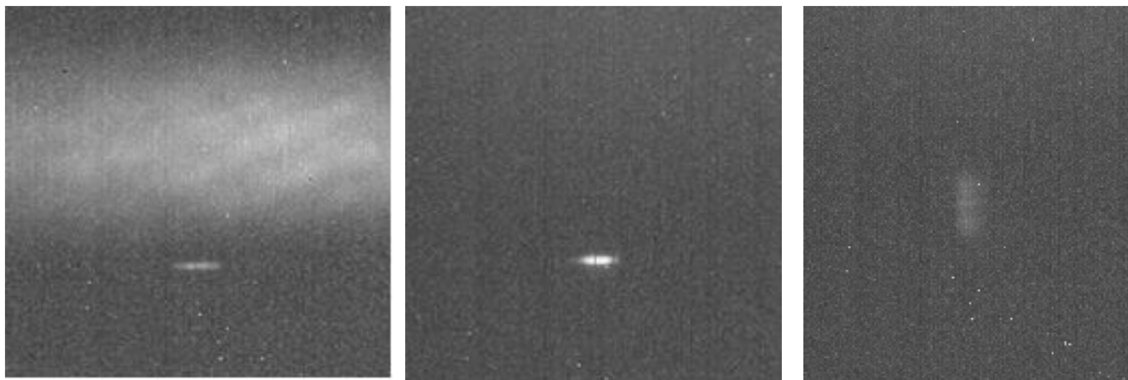

Figure 4.10: Light profiles from end facet of SM WG. When coupling starting (left), coupling moment (center), far field (right)

4.2.5 Results

When the simulation and experimental results compared, the mode profiles are similar. The design waveguide support only the fundamental mode (lateral and vertical). The dimension of coupled light which comes from end facet of waveguide is very close to the simulation results.

4.3 Single Mode Waveguides with Si_3N_4 Core with Lossy Layer

Si_3N_4 is very common material and easy to grow by PECVD with a refractive index higher than SiO2. So, instead of ZnO, Si_3N_4 can also be used as a core of waveguides. Previous ZnO based WG thickness was around 1.4 µm. So, it is very hard to locate the outgoing facet for the light. To determine the location of facet of the ridges, deep trenches are planned to be etches on both sides of the WG ridges.

The new waveguide structure has two Si_3N_4 core layers, which are vertically separated by a SiO_2 buffer layer. First, 20 µm wide and 5 µm ridges are etched into the silicon substrate. Then, the waveguides ridges are grown on top of these wider ridges.

A new mask has been designed to pattern the waveguides whose structure layers are given in Table 4.3. The details of the mask are given in Appendix B. The growth parameters for Si_3N_4 and SiO_2 are given in Appendix A, table A.1.

4.3.1 Waveguide Simulations

The waveguide should support only the fundamental mode both in lateral and vertical directions. Therefore, a rib of 7 μm wide has been etched by 300 nm to support only the fundamental mode laterally. The optical constants and thicknesses of the layers are given in table 4.3 and the device structure is shown in figure 4.11.

Table 4.3: Structure parameters of Si_3N_4 based SMW at λ = 1310 nm.

Layer	Refractive Index (n)	Thickness (μm)
Air	1.0	-
SiO_2	1.51	0.6
Si_3N_4	1.9827	0.4
SiO_2	1.51	1.0
Si_3N_4	1.9827	0.39
SiO_2	1.51	0.5
Ni	3.2 – 6.02i	0.1
Si	3.5	Substrate

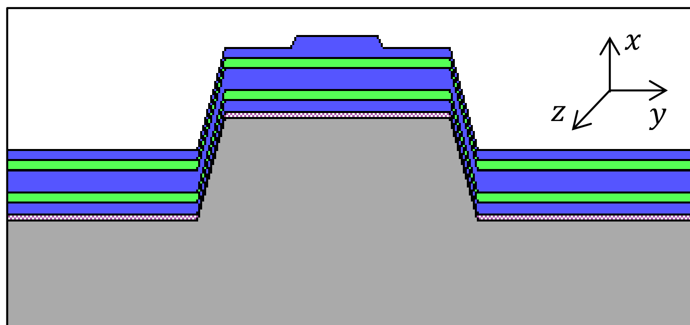

Figure 4.11: Cross-sectional view of single mode waveguides with Si_3N_4 core

For the structure along the vertical x-direction, TE and TM modes for the waveguide are calculated as shown in figures 4.12 and 4.13. This structure fabricated on

a silicon substrate and zero position for the mode profiles corresponds to the air boundary.

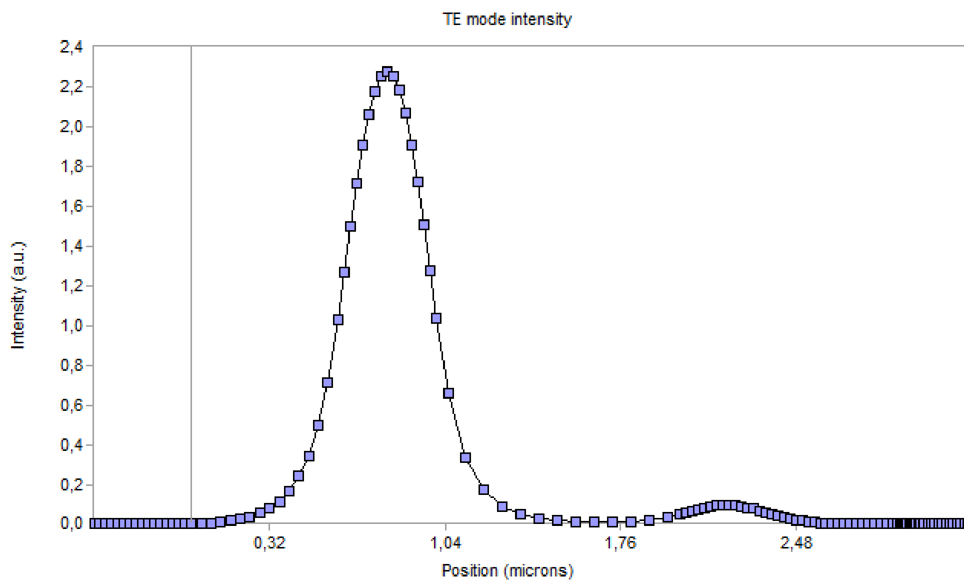

Figure 4.12: 1-D simulation of TE mode near field intensity

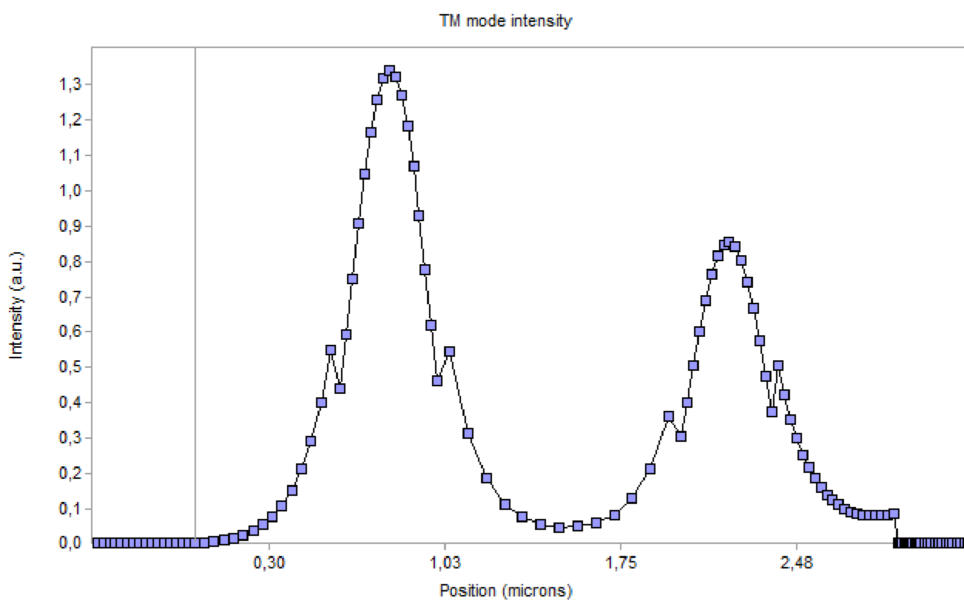

Figure 4 13: 1-D simulation of TM mode near field intensity

TE and TM even and odd modal losses with respect to thickness of bottom core Si3N4 layer are given in figure 4.14. The optical losses for the even TE mode, whose intensity profile is shown in figure 4.12, at a thickness around 390 nm is negligible

small (almost lossless). However, the other guided modes of the waveguide exhibit considerable optical losses at the same thickness. This can be seen from the intensity profile of the TM mode in figure 4.13, as an example. So, on the TE mode will propagate in the waveguide without experiencing losses when the bottom Si_3N_4 core layer selected as 390 nm.

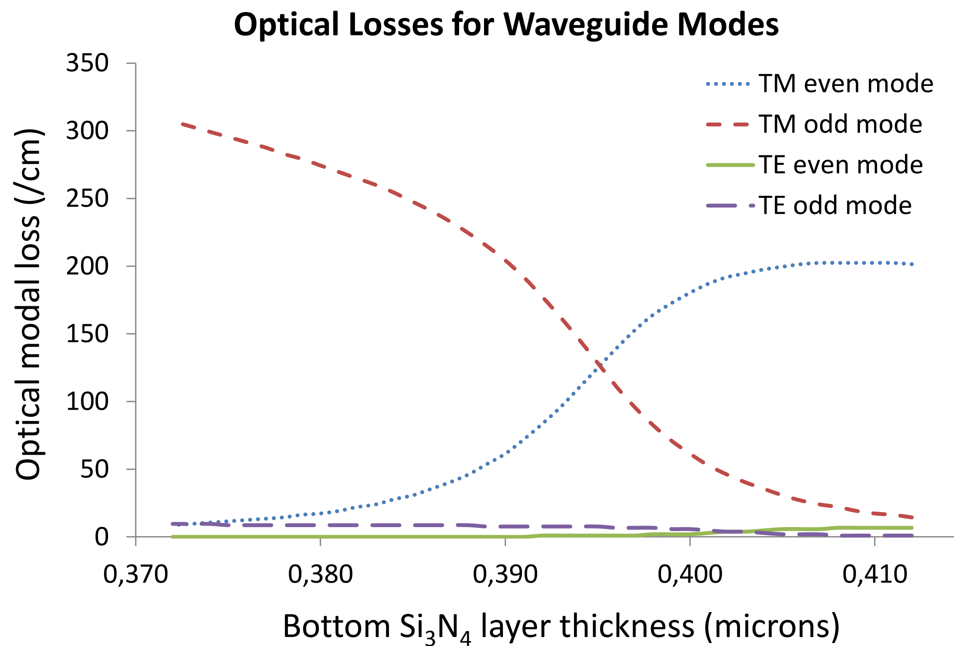

Figure 4.14: For TE and TM modes, optical losses of even and odd modes.

4.3.2 Fabrication Steps

The same chrome mask, which is mentioned in section 4.2, was used for fabrication of devices. As the first step, 20 μm ridges patterned on silicon substrate by wet etching with potassium hydroxide (KOH) solvent at 90°C for 5 minutes. Unfortunately, AZ5214 PR could not withstand during process. So, a SiO_2 was used as hard mask to protect ridges during deep wet etching process of silicon in KOH solvent. The procedure starts with growing a thin (150-200 nm) SiO_2 on silicon with PECVD. Then, it is patterned by PR using the same mask which consists of 20 μm ridges. Next, buffered-oxide-etch (BOE) solution was used for wet etching of SiO_2. After removing of photoresist with acetone, SiO_2 stays as hard mask while 5 μm deep wet etching of silicon in KOH solvent at 90 °C. After etching is done, SiO_2 hard mask was stripped out in BOE solution.

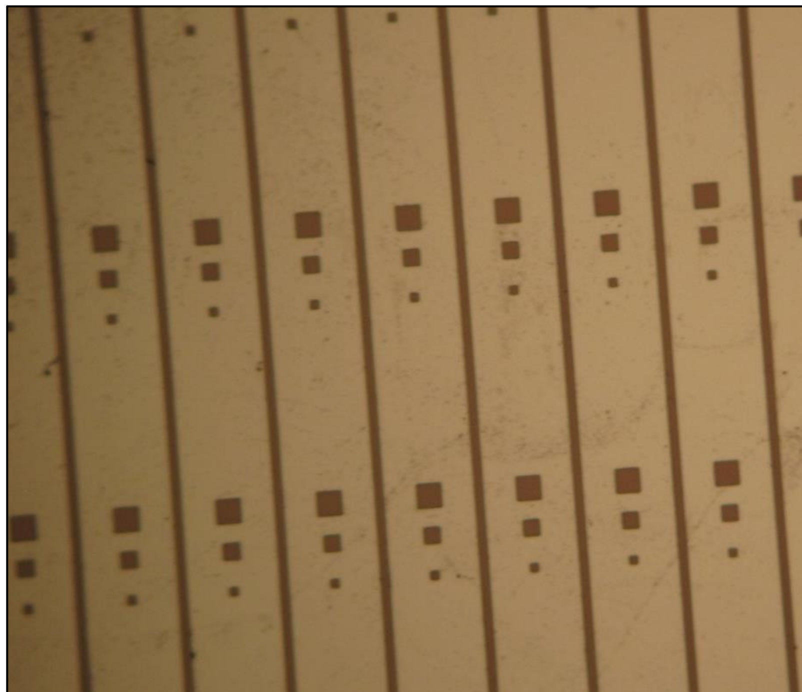

Figure 4.15: 2 minute deep wet etching of Si in KOH solvent at 90 °C.

Figure 4.16: SiO_2 hard mask removed after 3-minute wet etching of Si.

Figures 4.15 and 4.16 indicate that SiO_2 has well protected the desired areas. Even though etched surfaces with KOH on silicon is damaged, protected areas stayed clean and undamaged.

The layers in Table 4.4 were grown at the defined thickness. After the layers were grown, 7 µm wide ridges on the chrome mask were aligned as centered to the 20 µm wide silicon mesas. This step defines the waveguide ridges in which guided modes travel along the z-direction. Next, the top SiO_2 cladding layer was attempted to be dry etched by 300 nm in ICP and finally, PR was cleaned and samples were ready for the test.

The PR on the 20 µm wide mesa did not form well and the PR thickness was < 600 nm. Therefore, instead of the target thickness of 300 nm, SiO_2 came out to be etched around 190 nm. Also, some misalignment can be seen in figure 4.17, but this will not harm the guided modes in the waveguide.

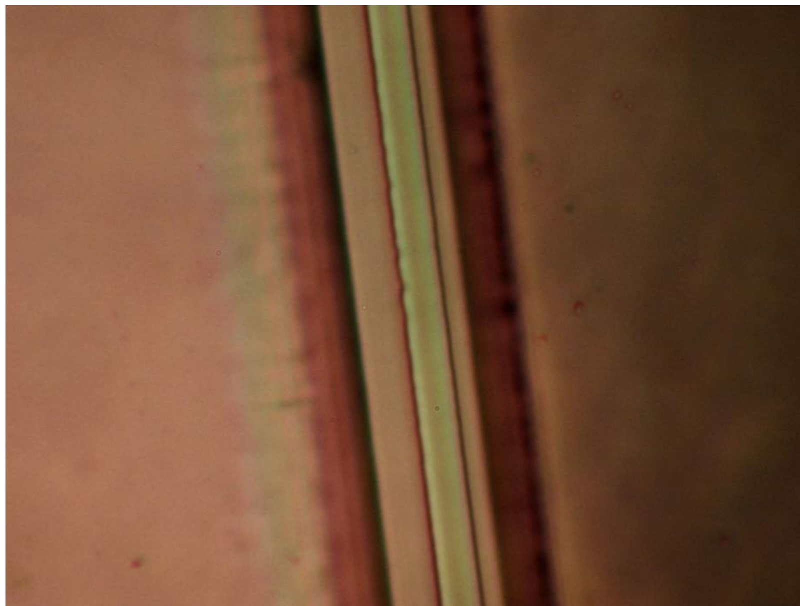

Figure 4.17: 100x microscope objective image of fabricated sample.

4.3.3 Experimental Findings

As shown in figure 4.18, coupled light travels along the z-direction and comes out from the end facet of SMW. The optical profile matches with simulated mode profile.

Also, the mode is not centered on the mesa which is an agreement with the misaligned ridge shown in 4.17.

Figure 4.18: TE mode near field intensity of coupled light into waveguide (40x objective)

The fabricated devices have been tested under TE and TM polarized light. First, a polarizer which is fixed in front of the laser was adjusted to 45° to allow both TE and TM polarizations at equal light intensities. With the help of a second polarizer which comes after the first polarizer, light intensity is measured by the detector for TE and TM polarizations. Light intensities for TE and TM polarized light came out to be equal.

When the second polarizer is adjusted to allow TE polarized light, light coupled into the waveguide becomes TE mode. Figure 4.19 shows the out coming light from the waveguide for TE mode. This is the fundamental mode profile. Then, the second polarizer was set to pass TM polarization without altering the coupling conditions. In this case, the light guided in the waveguide is the TM mode. Light coming out of the facet is shown in figure 4.20. The light is heavily attenuated and intensity is much lower compared to the TE mode case.

Referring to figure 4.14 again, the modal loss for the TE mode is negligible and it is considerable for the TM modes. The mode intensities shown in figures 4.12 and 4.13 also indicates that there is almost no light confined in the nickel layer for the TE mode, whereas significant amount of light is confined in the nickel layer for the TM mode. As a result, TE mode experiences no loss and TM mode is absorbed by the lossy nickel layer as it propagates. The devices tested here are about 6.5 mm long.

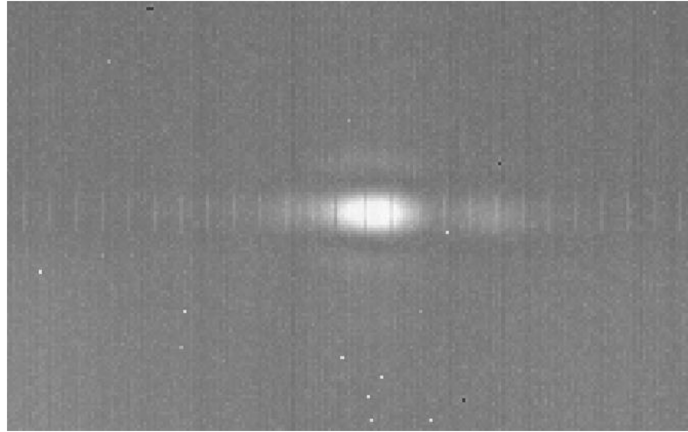

Figure 4.19: TE mode coupled into waveguide on fabrication completed sample (100x objective used to have better resolution)

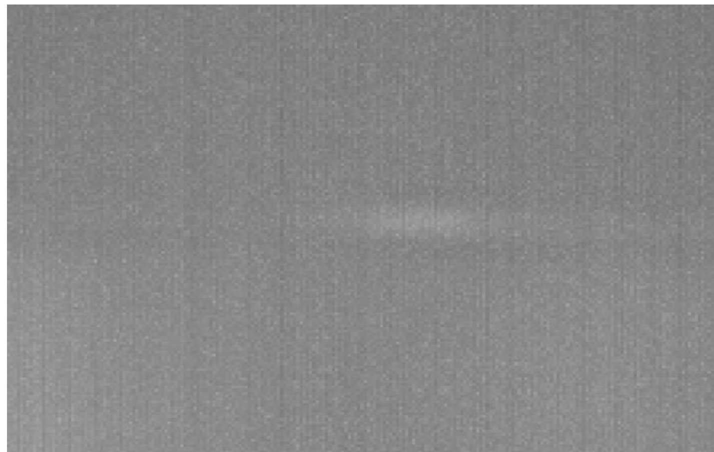

Figure 4.20: TM mode coupled into waveguide for another device on fabrication completed sample (100x objective used)

4.3.4 Results

In this section, polarization selective devices have been demonstrated, which allow TE mode to propagate without loss, but effectively attenuate the TM mode. The simulated modal intensity profiles and the intensity profiles obtained by the measurements confirm that these devices act as waveguide polarizers.

4.4 Design of an Optical WG Isolator with Si_3N_4 Core and Nickel Layer

In the previous section, waveguides were fabricated on silicon mesas with 20 µm width trenches on both sides. These trenches caused to appear multimode light which is most probably confined by air on both sides of silicon. Therefore, waveguides must not interfere with those trenches and mesas should be wide enough to prevent this interaction (~70 µm). A new chrome mask has been designed and the structure of waveguides has been modified.

In the new designed, there are again two guiding layer in the waveguide, which are two Si_3N_4 core layers. These guiding layers are vertically separated by SiO_2 buffer layer and the nickel layer will be on top. Bottom core Si_3N_4 and top cladding layer SiO_2 were etched to provide lateral confinement for single modes in both waveguides.

Besides straight ridge waveguides, there are waveguides with single ridge separating into four equal branches. Light couples into one ridge and after traveling 2 mm, it splits into two continuous parallel branches along the waveguides and again after 2 mm both branches split into further two continuous parallel waveguide branches. In other words, when light couples into the waveguide, for an ideal and lossless case, its intensity will be shared by %25 in four branches. These four waveguide branches have exactly the same bottom guiding layers at the bottom part.

The first branch was fabricated only with bottom waveguide and once the light is coupled to ridge, it will propagate as a single mode without any interaction. It does not have a top waveguide and a lossy medium. The second branch which was fabricated to examine of interaction between bottom and top waveguides has both waveguides. But there is no lossy media in this section. The third and fourth branches have an extra lossy nickel layer on top. The only difference between third and fourth branches is the length of lossy medium which is fabricated to the top of waveguide.

Since the guided light will separate equal intensities, after travelling through the ridges, the out coming light intensities can be compared. Most of the light is guided though the bottom waveguide and the top waveguide end before the output facet of the waveguide. This way only the light from the waveguide will be observed from the camera side.

4.4.1 Waveguide Simulations

The guiding layers in the waveguide will support only the fundamental mode both in lateral and vertical directions. For the bottom Si_3N_4 guiding layer, fundamental mode is provided by lateral confinement by forming a rib of 7 µm wide has been etched by 5 nm. As for the top Si_3N_4 waveguide section, a SiO_2 rib of 5 µm wide has been etched by 300 nm to support only the fundamental mode laterally. The optical constants and thicknesses of the layers are given in table 4.4 and the device structure is shown in figure 4.21. The mode profile for the structure is also shown in figure 4.22.

Table 4.4: Structure parameters of Si_3N_4 based optical Isolator at λ = 1310 nm

Layer	Refractive Index	Thickness (µm)
Air	1.0	-
Ni	3.2 – 6.02i	0.1
SiO2	1.51	0.6
Si3N4	1.9827	0.515
SiO2	1.51	0.5
Si3N4	1.9827	0.48
SiO2	1.51	0.9
Si	3.5	Substrate

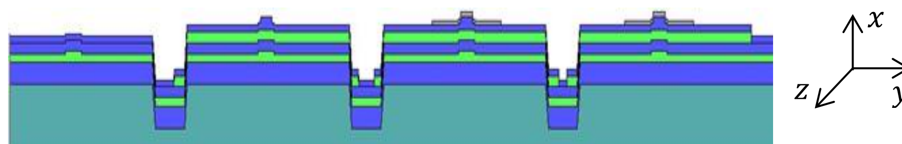

Figure 4.21: Cross-sectional view of single mode waveguides with Si_3N_4 core

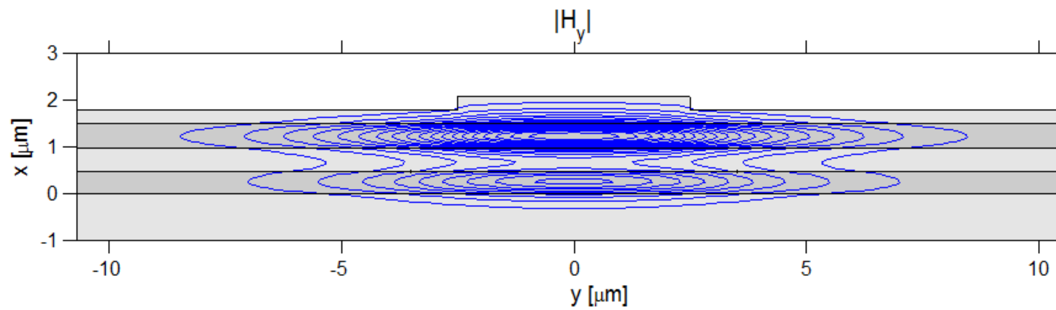

Figure 4.22: TM mode profile

4.4.2 Fabrication Steps

The layers were grown at the thicknesses shown in Table 4.4. A new mask was used to fabricate the structure which has two SMWs coupled vertically. The mask sections for fabrication steps are given in Appendix B. The device shown in Figure 4.21 was fabricated with the following steps:

1- 20 µm wide and 5 µm deep trenches were etched into silicon. Devices lay on the plateaus between the trenches.

2- The layers in Table 4.4 were grown.

3- The main waveguide at the bottom was fabricated by etching Si_3N_4 7 µm wide and 5 nm deep.

4- The mask section shown in figure B.3 was used to define the top Si_3N_4 waveguide.

5- The top SiO_2 layer was etched to form 5 µm wide and 300 nm deep ridges.

6- Finally, the nickel layer was defined using the mask section shown in figure B.6

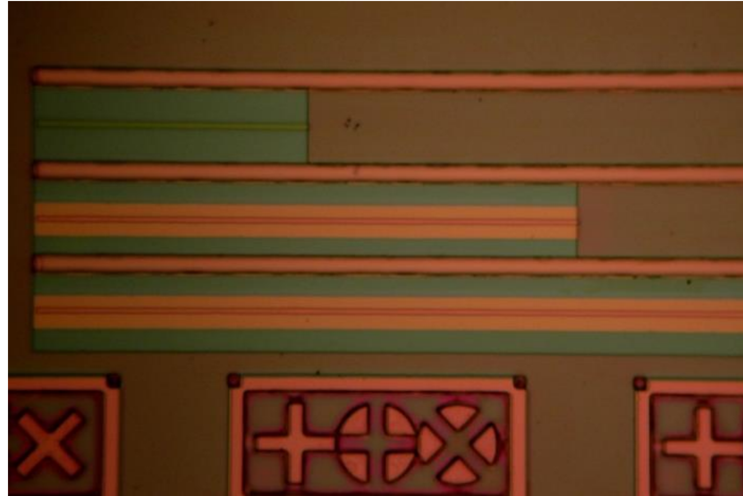

Figure 4.23: 20x microscope objective image of fabricated sample with four branches

The fabricated device sections are shown in figures 4.23 and 4.24. In figure 4.23, the thin stripes are the SiO_2 etched ridges and wide stripes along the ridges correspond to the top waveguide. The nickel stripes are on top of only the two branches, on the bottom side. Figure 4.23 is a close view of the ridges with nickel on top. The center ridge is etched SiO_2 ridge. The medium ridge is the nickel on top. The wide ridge is where the top Si_3N_4 waveguide stays.

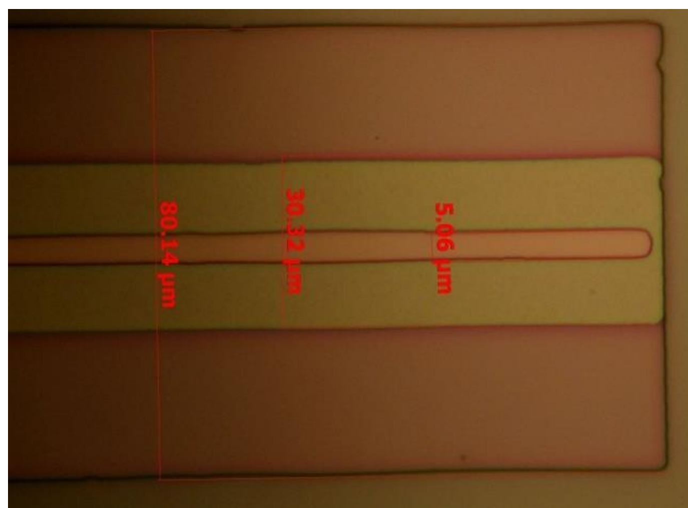

Figure 4. 24: 100x microscope objective image one of the branches of the fabricated sample with nickel on top

4.4.3 Experimental Findings

The fabricated devices have been tested to observe the out coming light coming from different branches. The TE polarized light is coupled in to the waveguide and figure 4.25 shows the light at the facets. The rightmost ridge contains only the bottom guiding section and single mode light is observed at this branch. The second ridge from the right has both waveguides but no nickel on top. Due to the interaction with the top waveguide layers, the intensity has decreased. The light intensity dropped significantly in the third and fourth (not shown in the figure). Therefore, the devices could not be tested under magnetic field due to high absorption of nickel.

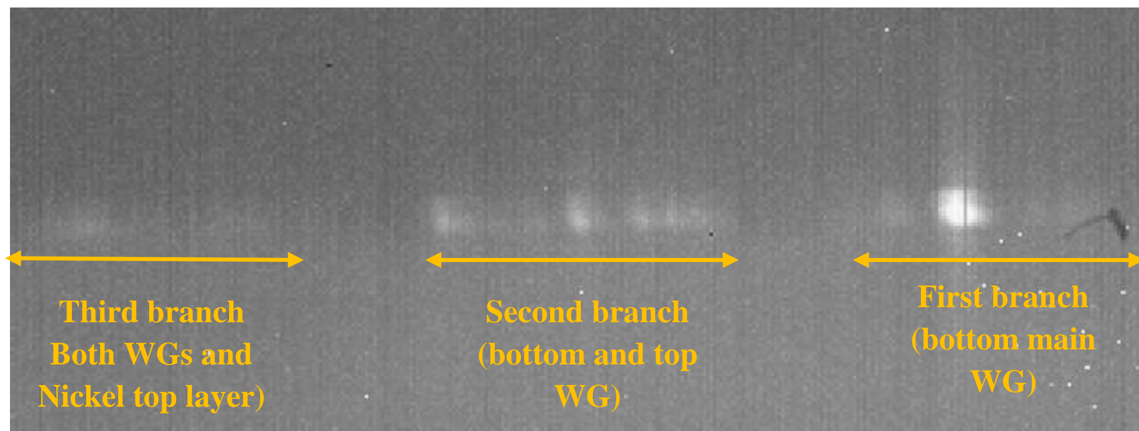

Figure 4.25: TE mode intensity profile coupled out of end facet of a device with four branches (40x image)

4.4.4 Results

As seen from figure 4.22 the light intensity in top guiding section for the mode is substantial. Therefore, the interaction of the light with lossy nickel has dramatically attenuated the light. Therefore, the confinement of light in the top layer should be decreased and also the loss in the top layer should be reduced by replacing nickel with a less lossy material

4.5 Design of an Optical WG Isolator with Si_3N_4 and ZnO:Ni Core

The results from the previous design show that the light confinement in the guiding layer should not be high and also nickel is too lossy. In this section, a composite

material which has lower optical losses but has magnetic properties has been characterized. This material is zinc oxide doped with nickel (ZnO:Ni), where nickel concentration is varied and optical constants for the films were measured. These composite films were grown with the parameters which are given in table A.2 in Appendix A.

The new waveguide structure has Si_3N_4 and ZnO:Ni core layers, which are vertically separated by a SiO_2 buffer layer. The mesa sections where the ridges are fabricated are very wide (1500 µm) to prevent the effect of trenches.

A new mask has been designed to pattern the waveguides whose structure layers are given in Table 4.5. The details of the mask are given in Appendix B. The growth parameters for Si_3N_4 and SiO_2 are given in tables A.2 and A.4, respectively.

4.5.1 Waveguide Simulations

The guiding layers in the waveguide will support only the fundamental mode both in lateral and vertical directions. For the bottom Si_3N_4 guiding layer, fundamental mode is provided by lateral confinement by forming a rib of 7 µm wide has been etched by 5 nm. As for the top ZnO:Ni waveguide section, a SiO_2 rib of 5 µm wide has been etched by 300 nm to support only the fundamental mode laterally. The optical constants and thicknesses of the layers are given in table 4.5 and the device structure is shown in figure 4.15. The mode profile for the structure is also shown in figure 4.27.

Table 4.5: Structure parameters of Si_3N_4 and ZnO:Ni based SMW at $\lambda = 1310$ nm.

Layer	Refractive Index	Thickness (µm)
Air	1.0	-
SiO_2	1.51	0.6
a-Si	3.5	0.007
ZnO:Ni	1.9142 – i0.00092	0.436
SiO_2	1.51	1.35
Si_3N_4	1.8992	0.485
SiO_2	1.51	2-3
Si	3.5	Substrate

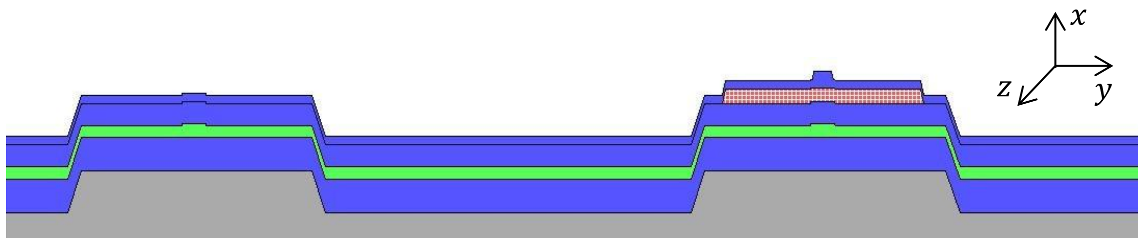

Figure 4.26: Two branch waveguide grown on silicon substrate, left branch is main bottom WG and right branch is ZnO:Ni WG on top

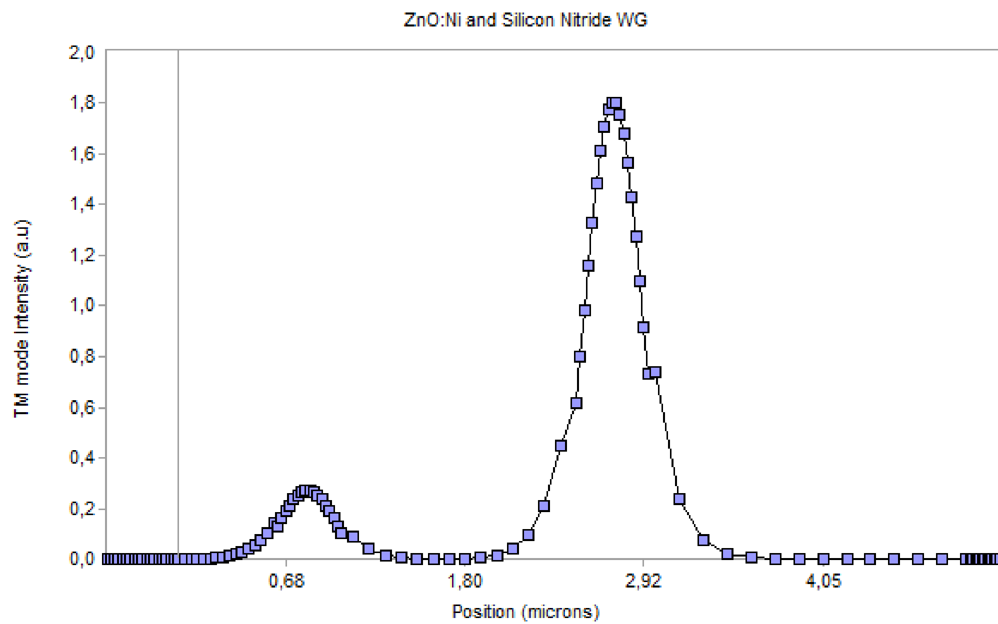

Figure 4.27: Optical intensity profile of TM mode for ZnO:Ni based WG

4.5.2 Mask Sections

Details of all the sections for the mask is given in Appendix B. Figure 4.28 shows two types devices. There is a straight ridge waveguide with a n interaction of ZnO:Ni regions indicated as rectangular areas. Another device is also a ridge waveguide with two branches. One branch has only the bottom guiding layers and the other one has an interaction region with ZnO:Ni top wave guiding layers.

Figure 4.28: The main bottom waveguide structure with two branches on mask

4.5.3 Fabrication Steps

The layers were grown at the thicknesses shown in table 4.5. A new mask was used to fabricate the structure which has two SMWs coupled vertically. Some sections of the mask section superimposed together are shown in figure 4.28. Detailed mask sections for fabrication steps are given in Appendix B. The device shown in Figure 4.26 was fabricated with the following steps:

1- 15-30 µm wide and 5 µm deep trenches were etched into silicon. Devices lay on the mesas between the trenches which are separated by 1.5 mm.
2- The layers in table 4.5 were grown.
3- The main waveguide at the bottom was fabricated by etching Si_3N_4 7 µm wide and 5 nm deep.
4- The top WG was formed by ZnO:Ni layer and it is only fabricated on one of the branches.
5- The top SiO_2 layer was etched to form 5 µm wide and 300 nm deep ridges.

The images from fabrication steps are shown in figures 4.29 – 4.31. Figure 4.29 shows the top ridges patterned by PR and large rectangles are where ZnO:Ni layer is. Figure 4.19 shows the final step of the fabrication, which is 300 nm SiO_2 wet etch by BOE. A completed device is shown in figure 4.20. Unfortunately, the final wet etch caused some damage to ZnO:Ni layer beneath the SiO_2 layer. BOE etches both oxides but ZnO was supposed to be protected by SiO_2 layer. One possible explanation may be that PECVD grown SiO_2 has pin holes where BOE has penetrated and attacked ZnO. As a result, the final ridges did not form properly and the ridges were partially disappeared. The final condition of ridges is seen in figure 4.31.

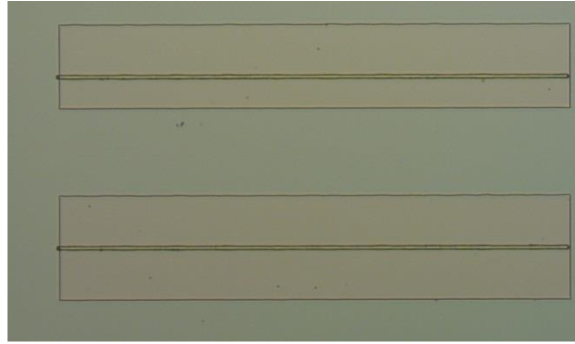

Figure 4.29: Patterned PR to form the 5 μm wide ridges on ZnO:Ni section

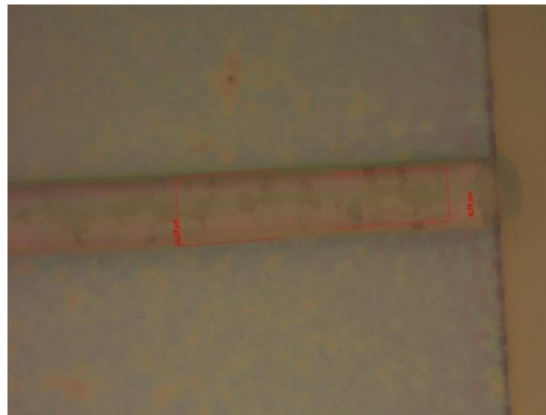

Figure 4.30: 100x microscope objective image of one of the ridges of the fabricated device (Before PR removed after BOE etching)

Figure 4.31: 100x microscope objective image of one of the ridges of the fabricated device (After PR removed and sample cleaned)

4.5.4 Experimental Findings

The fabricated devices have been tested to observe the out coming light coming from different branches. The TE polarized light is coupled in to the waveguide and figure 4.32 shows the light at the facets. The right most ridge contains only the bottom guiding section. The second, third and fourth ridge have ZnO:Ni top waveguide sections. Light comes out from the locations were the ridges are but it seems not to be well confined in the bottom waveguide sections because profile extends about 30 µm, instead of simulated ~15 µm.

The devices were tested under magnetic field to observe any changes in light intensity from the ridges. No noticeable changes were observed when magnetic field was applied or reversed. Either the modes do not interact with top layer (because they are not confined well at the bottom waveguide and light extends laterally, which reduces vertical interaction) or the ZnO:Ni layer cannot provide the magneto-optic effect considerably. They could be two reasons for this. One is that the nickel concentration (%5 for these devices) is not high enough; the other reason may be that the nickel is distributed in ZnO and is not magnetized, magnetic domains did not form. To form magnetic domains for magnetization, there should be a minimum size and this can be achieved by forming nickel islands or clusters. One solution can be annealing ZnO:Ni so that Ni atoms can aggregate.

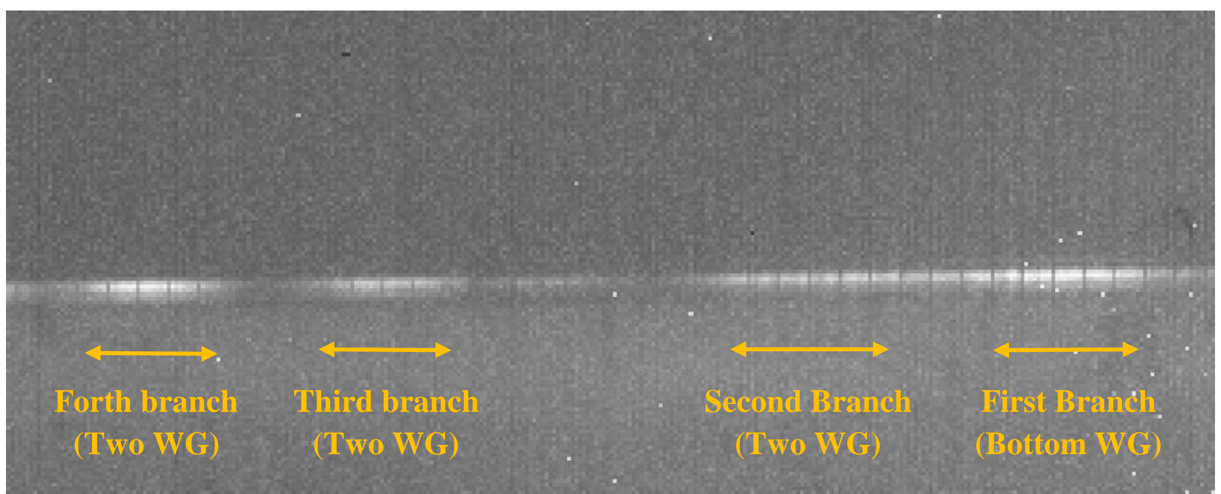

Figure 4.32: TE mode near field intensity profile of fabricated device with 100x microscope objective

CHAPTER 5

TEST SETUP FOR OPTICAL ISOLATOR

5.1 Experimental Setup

In this section, coupling experiment setup will be described and procedure of coupling process will be explained. Measurement setup consists of a 1310 nm (NIR) single mode laser as a light source, a collimator for collimating laser source light in front, two polarizers, one is positioned at 45 degrees to have equal light intensity for TE and TM polarizations and the other one is for selection of light polarization (TE or TM). There are two objective lenses in the setup, one is a wide range focal distance (0.2 mm) 100x lens for coupling the source light into the waveguide at and second wide range focal distance (7 mm) 40x to image the end facet of sample. On both sides of the sample, two magnet holders for NdFeB magnets are located, one of them is fixed and the other can move to change the magnitude of magnetic field. A beam splitter, to illuminate the end facet surface of sample under examination. The illumination source is a 1310 nm LED light with a nearly collimating lens. Two XYZ translation stages are used to carry and position the objective lenses for focusing and imaging. Finally, a 900 – 1700 nm wavelength rage InGaAs camera is used to capture the images of the coupled light at the end facet of cross section of sample with the help of wide distance 40x objective lens. Figures 5.1 and 5.2 are drawing of the experimental setup and figures 5.3 and 5.4 are the photos for the experiment

.

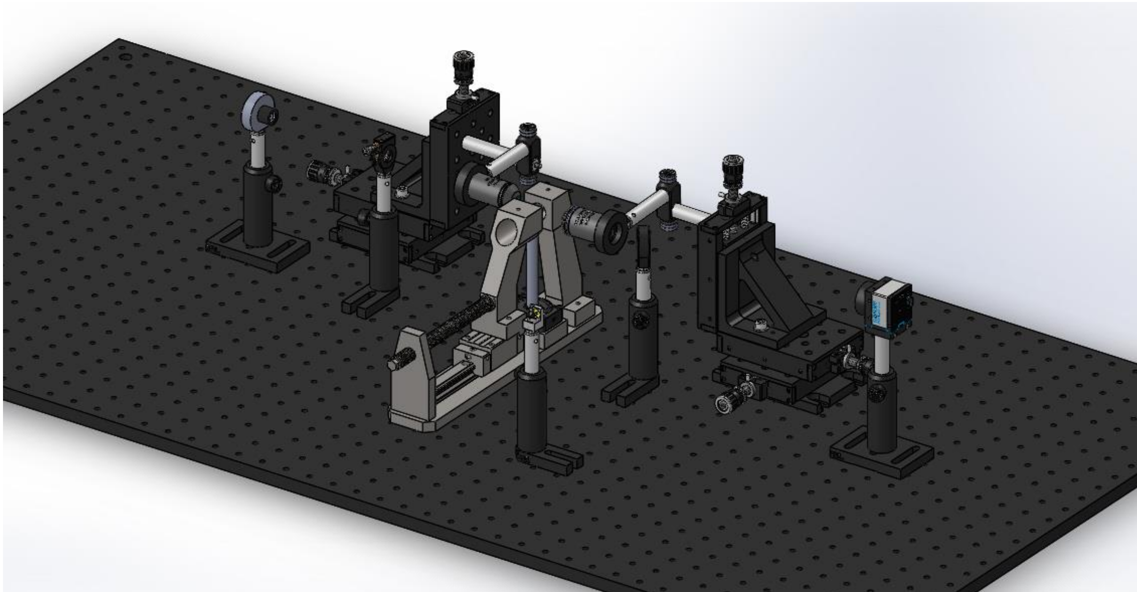

Figure 5.1: Coupling setup front right view

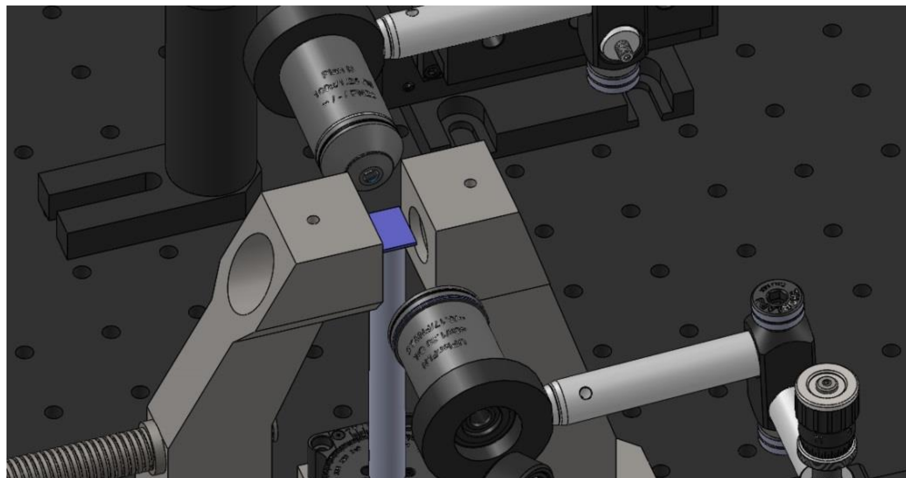

Figure 5.2: Close up view to the sample vacuum holder, magnet holder, imaging and coupling objective lenses

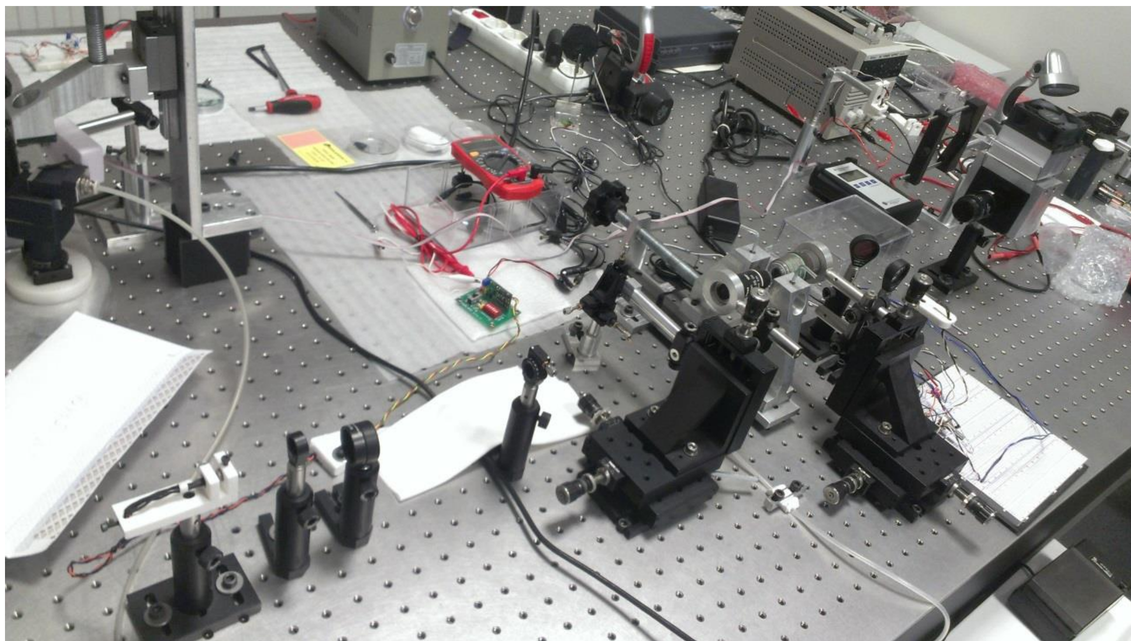

Figure 5.3: Coupling setup

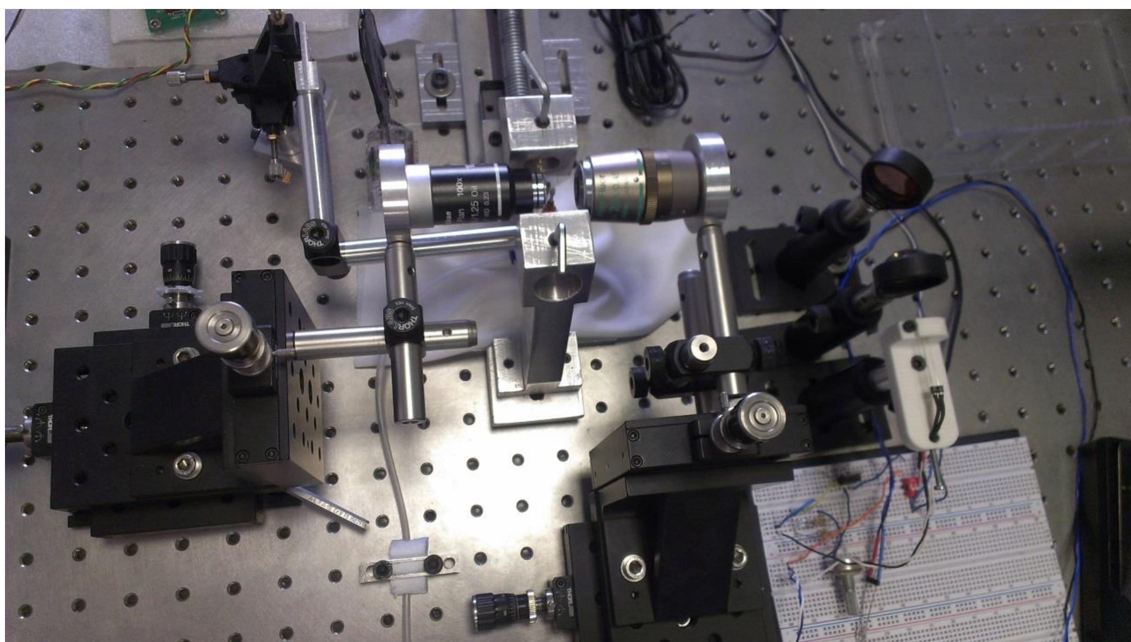

Figure 5.4: Close up view to the sample vacuum holder, magnet holder, imaging

CHAPTER 6

CONCLUSION

6.1 CONCLUSION

In this work, waveguides containing a Si_3N_4 core layer cladded by SiO_2 were fabricated on silicon and glass wafers and single-mode operation was observed. Next, double waveguide structures containing two Si_3N_4 core layers cladded by SiO_2 and a Si_3N_4 and ZnO:Ni core layers cladded by SiO_2 were fabricated to realize polarizers and isolator operation.

Some waveguides contain nickel (Ni) thin films and some contain ZnO:Ni composite films exhibiting magneto-optic Kerr effect (MOKE). The devices were designed for the isolator operation and utilized MOKE to allow the light to propagate in one direction and to absorb the light in the reverse direction. Waveguide polarizers exploiting the difference in the effective indices of transverse electric (TE) and transverse (TM) modes, were designed and fabricated. The behavior of modes propagating in the waveguides were investigated by 1-D WAVEGUIDE and 2-D WMM mode solvers.

The mask sets were designed for the fabrication processes of polarizer and isolator devices. The layers that constitute the structures were grown and optical characterization of theses film were made. Devices were fabricated in the cleanroom environment and tested on the coupling experiment setup to observe polarizer and isolator operation.

When tested under different polarization states of light, waveguide polarizer showed that light for TE modes can propagate without losses, TM modes are greatly attenuated. The waveguide isolators were designed for TM mode light to observe

change in light intensity under the magnetic field in opposite directions. However, no noticeable changes were observed when magnetic field was applied or reversed. The modes do not seem to interact with the ZnO:Ni magneto-optic layer. One possible reason is that the nickel concentration (%5) is not high enough to show the effect significantly; and the other reason may be that the nickel is distributed in ZnO is not magnetized because they did form magnetic domains. To form magnetic domains for magnetization, there should be a minimum size and this can be achieved by forming nickel islands or clusters. One solution can be annealing ZnO:Ni so that Ni atoms can aggregate.

APPENDIX A

Table A.1: Growth parameters for SiO_2 and Si_3N_4 on PECVD

Film	SiO_2	Si3N4
Base Pres. (Torr)	5E-5	5E-5
Working Pres. (Torr)	0.45	1
Substrate Temp. (°C)	250	250
Power (W)	10	9
N2O Flow Rate (sccm)	200	-
SiH4 Flow Rate (sccm)	200	200
He Flow Rate (sccm)	-	50
N2 Flow Rate (sccm)	-	75
NH3 Flow Rate (sccm)	-	4
Rate (nm/min)	12	4.25

Table A.2: Co-Sputtering Parameter for ZnO:Ni

Film	ZnO:Ni (95%:5%)
Base Pres. (Torr)	2E-6
Working Pres. (Torr)	4.5E-5
Substrate Temperature (°C)	Room Temp.
RF Power (W)	100
DC Power (W)	2
Rate (nm/min)	3.6
Ar Flow (sccm)	20

Table A.3: Wet etching parameters for fabricated materials

Material	**Etchant**	**Solvent Temperature**	**Rate**
SiO_2	BOE (NH_4F: H_2O 1:7)	Room Temp.	180 nm/min
Si	KOH:H_2O (2:6:1)	90 °C	1 µm/min
Si_3N_4	BOE (NH_4F: H_2O 1:7)	Room Temp.	13 nm/min
ZnO:Ni	HNO_3:HCl:H_2O (1:3:400)	Room Temp.	28.6 nm/min

Table A.4: Dry etching parameters for SiO_2 on ICP

Film	**SiO_2**
Base Pres. (Torr)	40E-3
Working Pres. (Torr)	20E-3
Substrate Temp. (°C)	40
ICP Power (W)	800
Coil Frequency (MHz)	13.56
O2 Flow Rate (sccm)	20
CHF3 Flow Rate (sccm)	100
Rate (nm/min)	19

APPENDIX B

Table B.1: 20 µm wide stripes on Mask - I

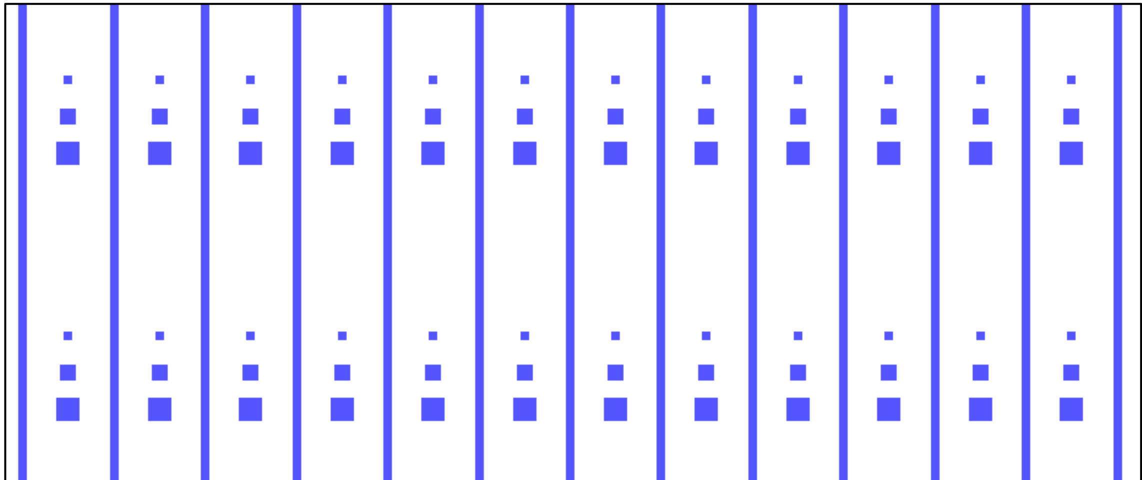

Table B.2: Trench section on Mask - II

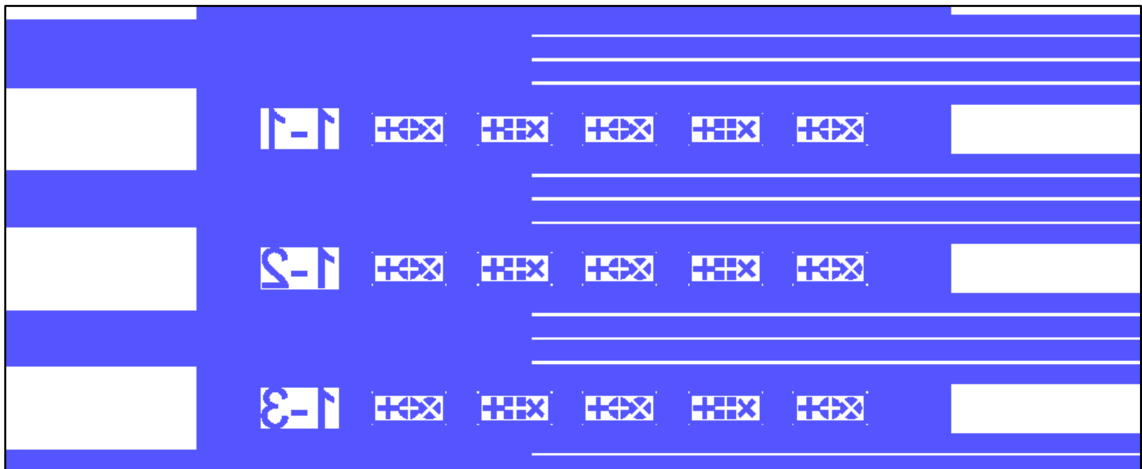

Table B.3: 5 nm deep, Si_3N_4-7 µm wide etch section on Mask - II

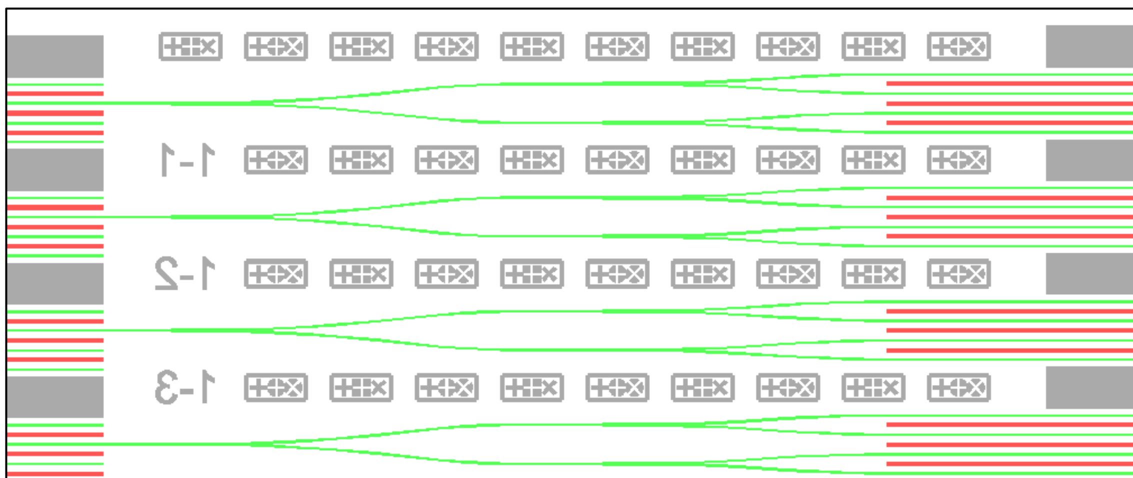

Table B.4: ZnO protection and etch section on Mask - II

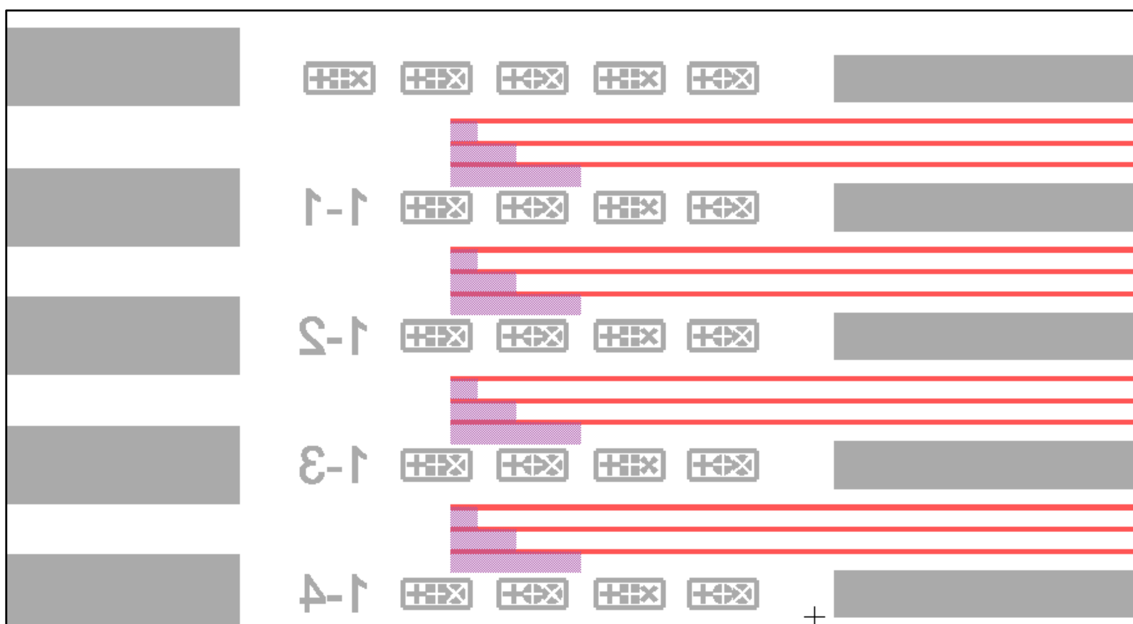

Table B.5: SiO_2 etch section on Mask - II

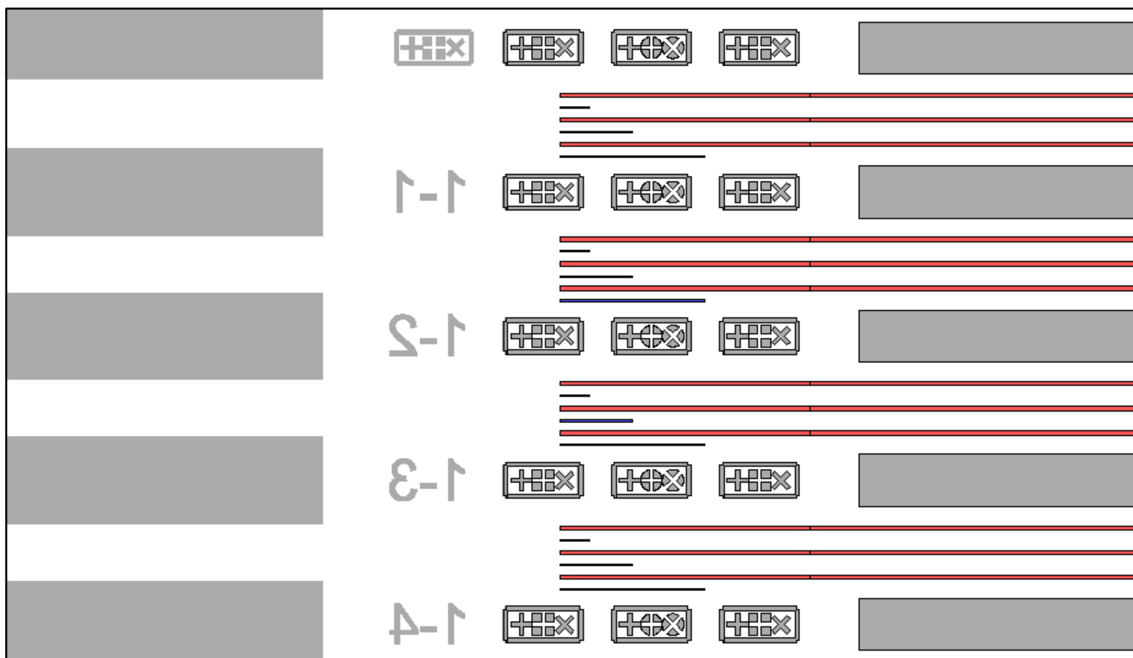

Table B.6: Nickel etch section on Mask - II

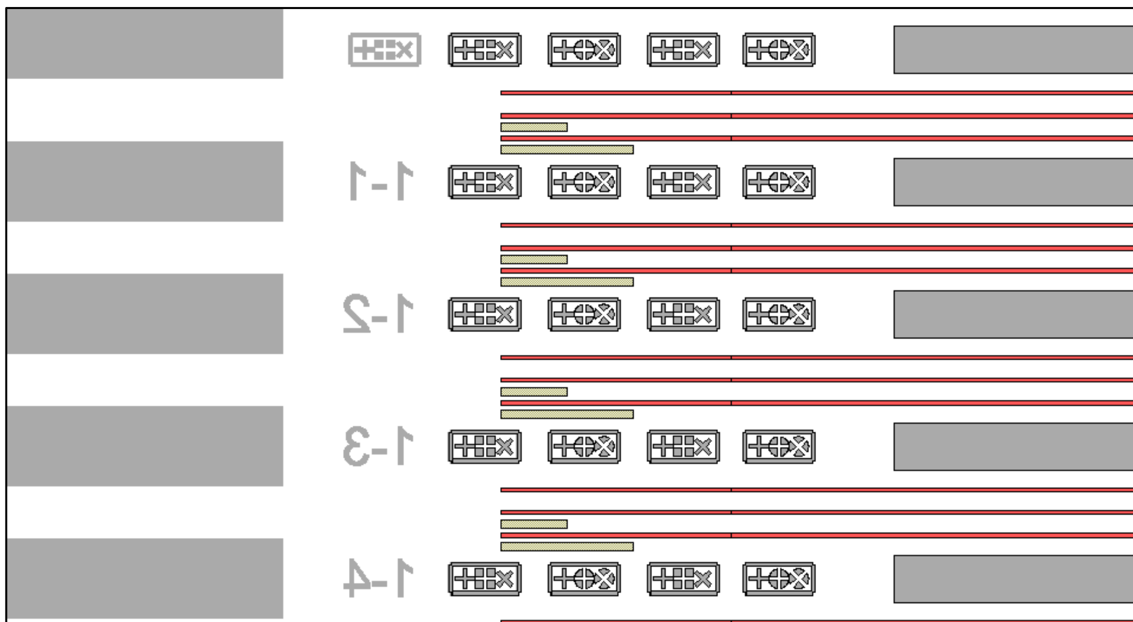

Table B.7: Trench section on Mask - III

Table B.8: Si_3N_4-5 nm deep, 7 µm wide etch section on Mask - III

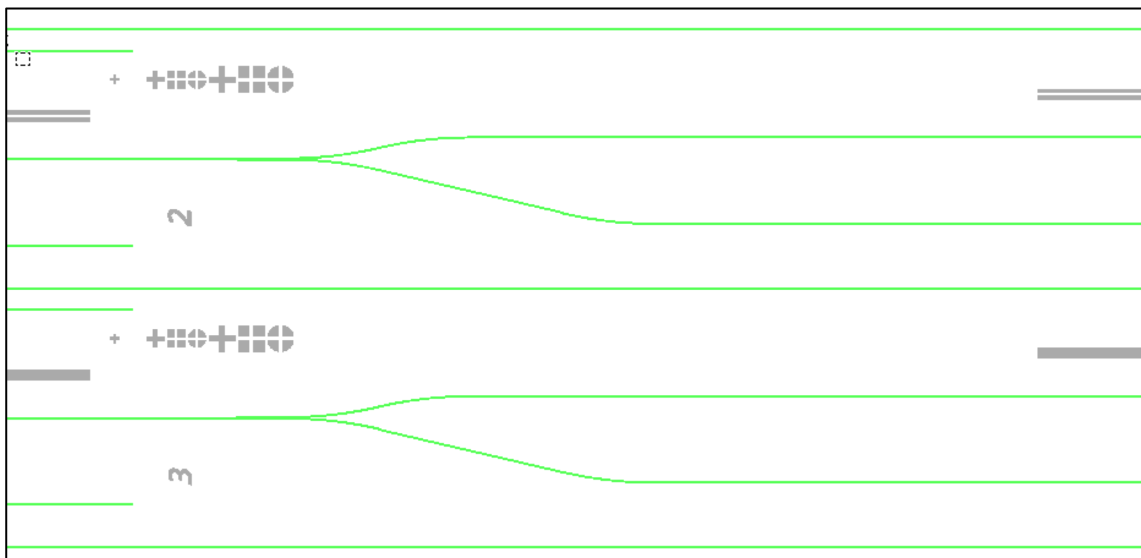

Table B.9: ZnO:Ni protection and etch section on Mask - III

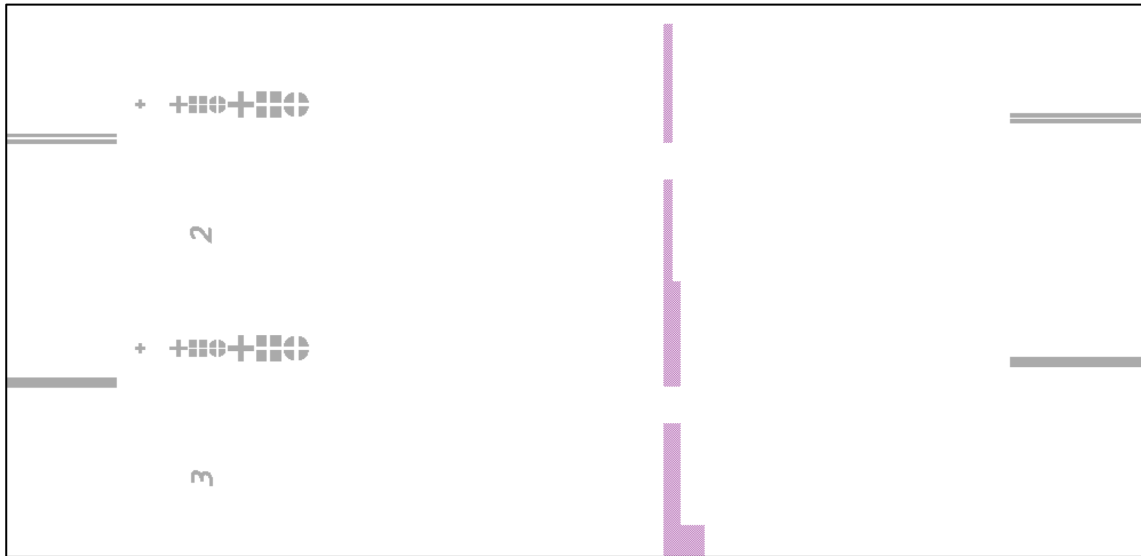

Table B.10: SiO_2 etch section on Mask - III

REFERENCES

[1] Infinera Cooperation, *Photonic Integrated Circuits A Technology and Application Primer*, 2006, http://www.infinera.com/pdfs/whitepapers/photonic_integrated_circuits.pdf.

[2] T. Hosking, *Optical Isolator Global Market Forecast and Analysis,* April 2014, http://www.electronicastconsultants.com/press.html

[3] G. Özgür, *Application of the Resonanat-Layer Effect to Integrated Isolators and Other Photonic Components*, PhD Dissertation, Southern Methodist University, 2005.

[4] I. Agha, M. Davanço, B. Thurston and K. Srinivasan, "Low-Noise Chip-Based Frequency Conversion By Four-Wave-Mixing Bragg Scattering in SiNx Waveguides", *Optics Letters*, Vol. 37, Issue 14, pp. 2997-2999, 2012.

[5] B. J. H. Stadler, T. Mizumoto, "Integrated Magneto-Optical Materials and Isolators: A Review", *Photonics Journal of IEEE*, Vol. 6, No. 1, February 2014.

[6] T. Tepper, F. Ilievski, C. A. Ross, T. R. Zaman, R. J. Ram, S. Y. Sung, and B. J. H. Stadler, "Magneto-optical properties of iron oxide films", *Journals of Applied Physics*, Vol. 93, No. 10, pp. 6948–6950, May 2003.

[7] K. Tanaka, K. Fujita, N. Matsuoka, K. Hirao, and N. Soga, "Large Faraday effect and local structure of alkali silicate glasses containing divalent europium ions", *Journal of Material Research*, Vol. 13, No. 7, pp. 1989–1995, July 1998.

[8] T.Mizumoto, Y.Naito, "Nonreciprocal propagation characteristics of YIG thin film", *IEEE Transections on Microwave Theory and Techniques*, Vol.MTT-30, No.6, pp. 922-925, 1982.

[9] M. Levy, "The on-chip integration of magnetooptic waveguide isolators", *IEEE Selected Topics in Quantum Electronics*,Vol. 8, pp. 1300-1306, November. 2002.

[10] H. Yokoi, T. Mizumoto, T. Takano, N. Shinjo, Demonstration of an optical isolator by use of a nonreciprocal phase shift, *Applied. Optics*, Vol. 38, pp.7409-7413, 1999.

[11] T. Mizumoto and Y. Naito, “Nonreciprocal propagation characteristic of YIG thin film", *IEEE Transections Microwave Theory and Tech*nology MTT-30, pp. 922–925, 1982.

[12] T. Mizumoto, S. Mashimo, T. Ida, Y. Naito, "In-plane magnetized rare earth iron garnet for a waveguide optical isolator employing nonreciprocal phase shift", *IEEE Transaction on Magnetics,* 29, pp. 3417–3419, 1993.

[13] H. Yokoi, T. Mizumoto, T. Takano and N. Shinjo, "Demonstration of an optical isolator by use of a nonreciprocal phase shift", *Applied. Optics*, Vol. 38, pp.7409-7413,1999.

[14] H. Yokoi, T. Mizumoto, N. Shinjo, N. Futakuchi, and Y. Nakano, "Demonstration of an optical isolator, with a semiconductor guiding layer that was obtained by use of a nonreciprocal phase shift", *Applied Optics*, Vol. 39, pp. 6158-6164, 2000.

[15] J. M. Hammer, J. H. Abeles, D. J. Channin, "Polycrystalline-metal ferromagnetic optical waveguide isolator for monolithic-integration with diode-laser devices", *IEEE Photonic Technology. Letters*, Vol. 9, pp. 631–633, May 1997.

[16] W. Zaets, "Optical waveguide isolator based on nonreciprocal loss/gain of amplifier covered by ferromagnetic layer", *IEEE Photonic Technology Letters*, Vol. 11, pp. 1012, 1999.

[17] K. Baba, F. Takase, and M. Miyagi, "Magnet-optic media composed of ferromagnetic metal island films for glass and semiconductor substrates", *Electronic Letters*, Vol. 32, pp. 222–223, Feb. 1996.

[18] J. M. Hammer, "Inline ferromagnetic-composite isolator and method", *U.S Patents*, Vol.6, pp. 760,496, July 6, 2004.

[19] J. M. Hammer, G. A. Evans, G. Ozgur, and J. K. Butler, "Isolators, polarizers, and other optical waveguide devices using a resonant-layer effect", *Journals Lightwave Technology.*, Vol. 22, No. 7, pp. 1754-1763, July 2004.

[20] M. Faraday, "Experimental Research in Electricity", *Philosophical Tranactions of the Royal Society London,* Vol. 136, pp. 1-20, January 1846.

[21] J. Kerr," On Rotation of the Plane of the Polarization by Reflection from the Pole of a Magnet", *Philosophical Magazine*, Vol.3, pp:321, 1877.

[22] M. Gaugitsch, H. Hauser, "Optimization of a magneto-optical light modulator Part-I: Modeling of birefringence and Faraday effect", *Journa of Lightwave Technology*, Vol.17, pp. 2633-2644, Dec. 1999.

[23] H. Fujiwara, "Spectroscopic Ellipsometry: Principles and Applications", *John Wiley & Sons Incorporated*, 2007.

[24] C.Y. You, S.C. Shin, "Generalized Analytic Formulae For Magneto-Optical Kerr Effects", *Journal Of Applied Phycis*, Vol. 84, No. 1, 1 July 1998.

[25] R. P. Hunt, "magneto-optic scattering from thin solid films", *Journals of Applied Physics* Vol.38, pp. 1652, 1967.

[26] J. Zak, E. R. Moog, C. Liu, S. D. Bader, "Fundamental magneto-optics", *Journals of Applied Physics*,Vol. 68, pp. 4203, 1990.

[27] J. M. Liu, "Photonic Devices", *Cambridge University Press*, Chapter 2, 2005.

[28] N. Litchinitser and V. Iakhnine, Optical Waveguide Numerical Modelling, http://optical-waveguides-modeling.net/mode-solvers-other-software.jsp#WMM.

[29] M. Hammer, Integrated Optics Modeling Group at the Department of Physics, *University of Osnabrueck,* 2000, http://wmm.computational-photonics.eu/index.html.